August 2018

In vivo, real-time spectroscopic assessment of contusion-based spinal cord injury in a rat model

Kyle Kelly Bishop
Syracuse University

Abstract

The goal of this study was to (1) develop a methodology for real-time, in vivo probing of chemical and physical changes in spinal cords and (2) compare these changes in the immediate aftermath of a localized contusive injury to uninjured spinal cords. Raman spectroscopy images were obtained on in vivo spinal cords that had been surgically exposed between T9 and T10. A total of six rats were studied in two n=3 groups of injured and uninjured control animals. A single 830 nm laser of 100 um round spot size was either spatially scanned across the cord or held at a specified location relative to the injury to improve signal to noise in the Raman spectra and explore effects of injury spread on surrounding tissue. Results show that Raman spectra acquired using our methodology show similar spectra to those acquired previously in our lab and with known literature. Principal component analysis was performed and showed three distinct components assigned to static tissue, cerebrospinal fluid, and plasma. Analysis of the Raman spectra suggest that the tissues underwent changes for both the control and injured animals; however, injured cords display Raman features indicative of changes known in spinal cord injury. Based on this work, use of Raman spectroscopy in the future could facilitate better understanding of in vivo injury in spinal cords.

In vivo, real-time spectroscopic assessment of contusion-based spinal cord injury in a rat model

by

Kyle K. Bishop

B.S. Bioengineering, Binghamton University, 2014

Thesis submitted in partial fulfillment of the requirements for the degree of

Master of Science in Bioengineering.

Syracuse University

August 2018

Acknowledgements

Firstly, I would like to acknowledge my advisor, Dr. Julie Hasenwinkel, for her patience, advice and guidance through this thesis work and my time at Syracuse University. Her willingness to help me through all of my numerous mistakes and failures through the years have helped me to grow as a researcher and I cannot thank her enough. I would also like to thank Dr. James Henderson for all of his advice and help through all of my work both in lab and as an individual. In addition, I would like to thank Dr. Chaiken for his knowledge and willingness to help through the entirety of this project, Seth Fillioe for his patience and help with the technical aspects of the work, and Alexander Vincent Struck-Jannini for all of his help with the animal surgeries and preparation. Lastly, I would like to thank my mother, Donna Bishop, my father, Charles Bishop Jr., and the rest of my family, without whom I would never have had the full support I needed to get this far in my life and whose love I cherish dearly; this work is your work as well.

TABLE OF CONTENTS

LIST OF FIGURES AND TABLES

Chapter 1: Introduction

Spinal cord injury (SCI) is a debilitating condition that affects approximately 347,000 people in the United States alone at a given time. More than half of the individuals with SCI are single at the time of injury, resulting in additional care being required, and those who are married see higher divorce rates over time. Even worse are the effects on employment, with approximately 12 percent of patients employed after being injured[1]. Although various levels of spinal cord injury exist, they all maintain the same effect of reducing the quality of life of the individual. Emotional, physical, and monetary pain is involved in SCI, leading to a great drive to understand how and what is occurring during the damaging process. Research is continually yielding more information about the state of the spinal cord after injury in an attempt to reduce or reverse the effects. In general, the effects of an injury can be seen as a physical disruption of the healthy tissue, resulting in a number of factors such as immediate neuronal death[2], glial cell phenotypic and functional changes[3], and endothelial cell death[4] resulting in cellular constituents, fluids, and the introduction of foreign matter not normally present in the spinal cord environment.[5] One primary concern is tissue changes early after injury. Understanding the effects of tissue change both in the injury area and in surrounding tissue could help lead to lessened hospital stay and possible reduction of the severity of injury.

Two events follow the aftermath of a spinal cord injury known as the primary phase and the secondary phase. The primary phase involves the immediate damage associated with injury such as cell lysing and tissue death. This leads to the secondary phase of injury, where nearby tissue becomes vulnerable to further degradation through a series of chemical and inflammatory events[6]. Bleeding can occur due to ruptured blood vessels and the breakdown of the blood-brain barrier exposes neuronal cells to ion imbalances, disruption of myelin function, and possible

infectious agents found in blood[7]. The secondary phase also involves migration of cells such as neutrophils and macrophages as well as cerebrospinal fluid leakage in and out of the damaged area, resulting in an even more complex environment than initially perceived[5,8].

Additionally, changes also occur within the tissue after injury. Astrocyte phenotypes are converted from passive to active and begin the process of glial scar formation, chondroitin sulfate proteoglycan (CSPG) chains are formed that inhibit neuronal regeneration, and microglia take on an ameboid-like phenotype that is similar to infiltrating macrophages[9,10]. Phagocytosis of myelin and apoptotic debris combined with neutrophil persistence in the area resulting in continued release of inflammatory cytokines can cause continued damage to surrounding bystander cells from early injury to even after glial scar formation[6,11].

Despite seeing these early effects of spinal cord injury on the tissue, more understanding is needed at the early timepoint after injury. Many currently available techniques to image changes in spinal cord tissue do so on a macro scale and are unable to differentiate chemical or cellular scale changes. Even though microglia are known to phenotypically change to resemble macrophages, this same mechanism makes their function after injury ambiguous due to difficulty in discerning between the two cell types[12]. The earliest imaging changes that occur can be seen using magnetic resonance imaging (MRI) and computer tomography (CT) scan, however both scans require hemorrhagic lesions to assess damage to the area[13]. In the case of a contusion style injury, where the trauma often restricts blood flow into the site, the effectiveness of these imaging modalities is severely limited[14,15]. In addition, while these methods can help visualize blood pooling in acute injuries, they cannot aid in visualizing the full area of injury, as many surrounding cells are affected away from the injury site, nor can they differentiate between the different types of tissue being affected[16]. The timeline of cell responses after injury is becoming

increasingly important to create clinical methodologies for treatment as well. Patients who undergo surgical repair after 24 hours tend to show a greatly decreased rate of recovery compared to those receiving early treatment[17].

To address these concerns, this initial study has developed a method of measuring early biochemical changes in spinal cord injury using Raman spectroscopy. Raman spectroscopy is a noncontact, nondestructive optical technique using scattered light from a sample to measure the chemical composition of the material[18]. A laser of known wavelength is focused onto a sample in the absence of external light sources. Molecules within the sample become excited and emit four waves of energy: Raleigh scattering, Fluorescence scattering, Stokes and anti-Stokes Raman scattering. Raleigh scattering involves an elastic energy transfer of the energy in the laser to the material, resulting in a wavelength returned at the same energy level as the laser[19]. Fluorescence scattering is the result of absorbed energy that emits photons over time in the sample and is commonly understood as noise for the purposes of Raman spectroscopy[20]. Stokes and anti-Stokes scattering are inelastic, near instantaneous changes in the energy state of a molecule. The resulting energy change results in the emission of a specific wavelength of energy correlated to the molecule[21]. Unlike the previous two scattering events, Stokes and anti-Stokes changes in energy are specific biochemical markers and can be used to determine the composition of the sample being measured[18,21].

A wide variety of utilizations for Raman spectroscopy have been demonstrated in both the medical and non-medical fields. Applications include scanning for measurements of the internal temperature of combustion engines[22], uses in the detection of precancerous and cancerous tissue[23], and determining the brittleness of bones in mouse models[24]. Additional work has been performed for in vivo measurements including the real time acquisition of gastric cancer

diagnosis during colonoscopy exams[25] and assessment of atherosclerotic plaques during femoral bypass surgery[26]. The different uses for Raman spectroscopy show how varied its applications can be. Recently, interest has been shown in the field of neurology, with studies ranging from tumor detection to cancer diagnosis in a neurosurgical environment[27,28].

Raman spectroscopy has been previously used in spinal cord studies in both an in vitro and ex vivo environment. Biochemical changes of ex vivo intact, injured spinal cord samples have been compared previously to uninjured spinal cords at time lengths of up to 8 weeks, showing differences in Raman spectra at each timepoint measured[5]. In vitro organotypic slices of spinal cord were analyzed using Raman spectroscopy to measure biochemical differences in tissue before and after use of chondroitinase ABC, a treatment method for spinal cord injury[29]. Results for both showed significant differences in many factors, such as changes in lipids, amide and protein content, and glycosaminoglycan concentrations over time. These timelines and resulting changes correlate with known literature results in spinal cord injury[6,14,30], however, there were limitations to these studies. Both used ex vivo spinal cord measurements to assess injury severity and could only measure at discrete timepoints after removal from the animals. In vivo, injury effects are dynamic processes that are difficult to measure once removed from the subject. In addition, increased interest in spinal cord tissue has helped to create a base of known wavenumbers established in literature to compare measured signatures in Raman spectroscopy to previous work[31–33]. Unfortunately, there is a lack of biochemical information on in vivo spinal cords using Raman spectroscopy, resulting in databases on biochemical markers being incomplete for in vivo work.

Using Raman Spectroscopy as a real time, in vivo measurement tool, this work measured chemical changes before and after contusion injury on the spinal cord tissue of rats. Surgery was

performed to expose the spinal cord by removing the dorsal half of the vertebrae and an impactor rod was dropped to simulate contusion injury. Three animals were used in injury testing, while three control animals only underwent the surgical procedure without the contusion injury. All subjects were scanned for a total of 5 hours after injury and spectra were compared to verify whether Raman spectroscopy could be used as an in vivo technique. Principal component analysis was used to visualize changes from injured to control animals, and wavenumbers that correlate to constituents within the tissue based on known tissue reactions to injury are discussed.

Specific Aims

Aim 1: Develop a method to acquire in vivo Raman spectra in spinal cord tissue over time for both injured and uninjured rats.

Aim 2: Compare the effects of contusion injury in spinal cord by location and time on in vivo Raman spectra to known literature of spinal cord injury.

Aim 3: Compare changes in specific chemical groups from Raman spectra to known tissue injury response to determine early biological reaction in spinal cord tissue following contusion trauma.

Chapter 2: Materials and Methods

2.1 Surgery and Animal Preparation

The animal protocol used was approved by the Institutional Animal Care and Use Committee (IACUC) of Syracuse University in compliance with National Institute of Health (NIH) guidelines. All surgical procedures were performed in a sterilized surgical suite located in the Laboratory Animal Research (LAR) facility at Syracuse University. Six female Sprague Dawley rats, at weight range 250g to 330g, were purchased from Charles River laboratories and housed in LAR at least two weeks prior to surgery to acclimate to their environment. Unless specified, all materials were obtained by ThermoFisher.

Animals were anesthetized using a procedure standardized in LAR for rat surgery with approval by a certified veterinarian. After placing the animal into a sealed chamber, 5% isoflurane (Shopmetvet, Mettawa, IL) was allowed to flow for 2 minutes until animal responses were minimal. After initial anesthetization, the animal was removed from the chamber and a nosecone was used to continually flow 2% or 2.5% isoflurane throughout the procedure depending on the weight of the animal. The surgical area was shaved and sterilized using alcohol and betadine-soaked pads. A hot water therapy pump (Braintree Scientific, Braintree, MA) was used to regulate the temperature of the animal throughout the procedure and was placed at 37^{o}C. The device was turned on prior to anesthetization to allow adequate time to reach temperature. All surgical tools were sterilized using a micro glass bead tabletop autoclave for 2 minutes per manufacturer instructions to ensure sterility before, during and for cleaning after surgery.

The locations of vertebrae T8, T9, T10 and T11 were verified through touch along the animal spine as both T8 and T11 spinal processes were more pronounced than surrounding

vertebrae. A final check was made to ensure deep anesthetization by tail pinch and blink reflex tests detailed in IACUC requirements. An approximately 1-inch long incision was made along the spinal column from T8 to T11 using a #10 scalpel blade (Fine Science Tools, Foster City, CA). A hole was cut into the fat layer beneath the skin using surgical scissors (Fine Science Tools, Foster City, CA) and blunt dissection was used to separate the muscle and fat layers; the fat layer was then cut and moved away from the surgical area. In parallel, incisions were made through each of the three muscle layers on either side of the spine. Once more, the position of the spinal processes was used to verify the location of T9 and T10 by moving the back of the scalpel along the vertebral column; incisions were made perpendicular to the spine between T8 and T9, T9 and T10, and finally T10 and T11. Muscle was gradually dissected using both surgical shears and a scalpel to expose bone. The dorsal layer of bone for T9 and T10 was removed to expose the spinal cord to a full length of at least 1 cm using Friedman-Pearson Rongeurs (Fine Science Tools, Foster City, CA). The area was cleaned using a saline spray and sterile cotton balls prior to scanning. After completion of the experiment, all animals were humanely euthanized under anesthesia through an overdose of 0.5ml pentobarbital (Sigma-Aldrich) by intraperitoneal injection.

2.2 Impactor Device

The injury model for a rat and all techniques for creating a contusion injury were developed by Rutgers University's W.M. Keck Center for Collaborative Neuroscience division[30]. The contusion injury for all injured animals was produced using the Multicenter Animal Spinal Cord Injury Study (MASCIS) Impactor model III using the standard 3mm size impaction tip at 12.5mm above the spinal cord. These parameters have been previously shown to induce a

moderate level of spinal cord injury. All animals were aligned beneath the impactor regardless of injury to ensure any additional factors in moving after surgery were accounted for.

2.3 Micromotor Stage and Raman Alignment

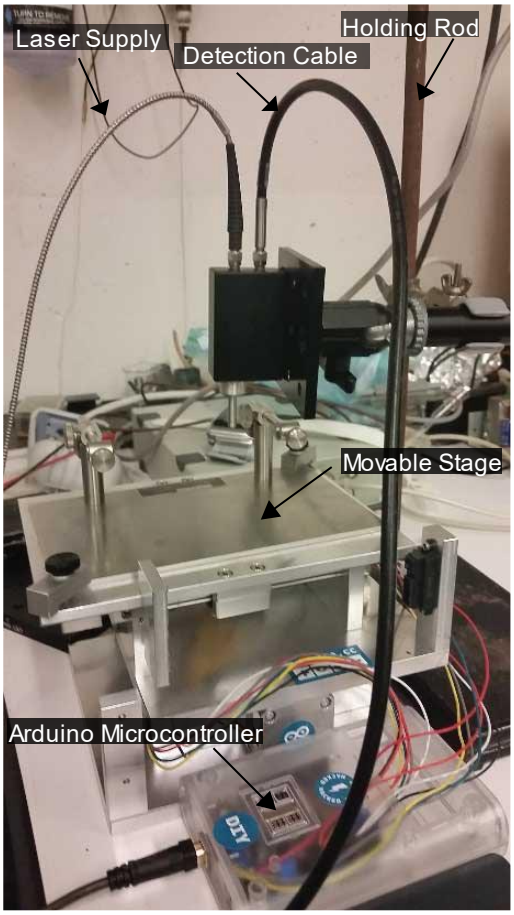

Figure 1: Diagram showing the X-Y stage with Raman laser above the animal clamps. The black box is the Raman laser housing, with the silver cable supplying the laser and the black cable connecting to the detector. The moveable stage is controlled by an Arduino micromotor to move beneath the laser housing without changing the laser position.

In order to scan across the spinal cord of the animal, a programmable x-y stage was developed in the Hasenwinkel lab shown in Figure 1. An Arduino microcontroller, using a custom-built MATLAB script, was capable of controlling two separate stepper motors independently with steps as small as 10 microns. An additional fixed arm was attached in order to hold the Raman laser in place. The arm was placed on the stationary portion of the stage, allowing the stage to move beneath the laser. After the surgical procedure, the animal was carefully moved to the stage to avoid agitating the surgical area. Two vertebral clamps on the stage platform were attached to T8 and T11 to minimize animal movement during scanning. This also allowed the spinal column to be aligned in a single dimension to maintain scanning across the spinal cord. Both the stage and the MASCIS impactor were placed onto a table with black drapes placed on struts to prevent external light in the room from reaching the Raman laser.

To verify weight-drop location on the cord, the top of the stage was modified to include a rail that extended out underneath the MASCIS impactor. The Raman laser was focused manually before the animal was carefully moved along rails attached to the stage until underneath the MASCIS impactor. Three positions were determined at this time along the spinal cord in reference to where the impact of the weight occurred, denoted as position A, towards the rostral end of the animal, position B, on the center of the weight drop, and position C, towards the caudal end of the animal as depicted in Figure 2. Both positions A and C were located a distance of 1-millimeter away from the spinal column on either side to avoid potential overlap with bone, where the approximate distance for position B would be centered between positions A and C to determine drop location. Once the positions were determined, the animal was returned along the rail to the stage and secured. The Raman laser spot size was re-verified before beginning the scanning process.

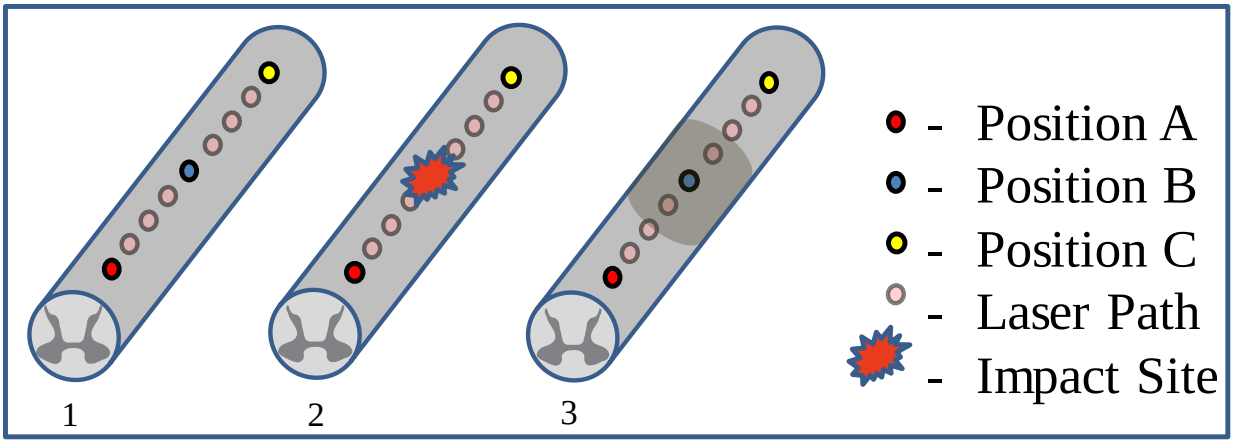

Figure 2: Schematic of experimental injury. 1). Spinal cord before injury and the normal scan path of control experiments. 2). Approximate impact site of the injury. 3). Spinal cord after contusion injury. Darkened area shows the immediate vicinity of impactor drop. Each position was scanned for 5 minutes before spending 5 minutes moving to the next position beginning at position A. After all points are scanned the laser returned to its starting position.

2.4 Raman Scanning Method

After verifying the positions on the cord, all light sources were turned off and the room was made dark with the exception of a monitor to see live Raman spectra acquisition. A black

tarp was placed over the animal, stage and impactor to ensure as little exterior light as possible reached the Raman detector. In order to maintain equal scanning times for each of the three positions along the spinal cord and avoid potential burning from prolonged exposure, a set scan time of 25 minutes was used for one complete scan and can be visualized in Figure 2. Within this timeframe, the detector remained on one position, beginning with position A, for 5 minutes. The stage was then moved over the course of five minutes to the next location to scan across the distance between position A and B. Upon reaching position B the stage was stopped for 5 minutes of scanning with the process being repeated for the distance between positions B and C. Once the scanning process was complete, the stage returned to the initial position and the animal was monitored to ensure adequate hydration of the injury site as well as continued respiration and anesthetization were maintained throughout the procedure. This procedure was completed a total of 10 times for all animals over the course of five hours.

2.5 PV[O]H Algorithm and Hematocrit Mapping

A specialized algorithm developed by Dr. Joseph Chaiken's lab was used to determine hematocrit levels in the spinal cord during Raman scanning. All backscattered light is created using a near infrared laser and can be categorically separated into two states: elastically scattered light (EE) equivalent to Rayleigh light scattering where no energy is lost between collection and collected light with a wavelength shift denoted as inelastic light scattering (IE). We modeled the spinal cord as a three-phase system consisting of red blood cells, plasma volume and static tissue, and also assumed that the tissue had no voids. Based on the optical scattering of those features, volume fractions of these characteristics can be developed as shown in Chaiken et. al.[34] Hematocrit (Hct) was defined as shown in equation 1, with red blood cell volume fraction (ϕ_r) defined in equation 2 and plasma volume fraction (ϕ_p) shown in equation 3.

1. $Hct = \phi_r/(\phi_r + \phi_p)$
2. $\phi_r = a + b\left(\frac{EE}{EE_0}\right) + c(\frac{IE}{IE_0})$
3. $\phi_p = d + e\left(\frac{EE}{EE_0}\right) + f(\frac{IE}{IE_0})$

The six parameters, a through f, are values determined from previous results on capillary blood in skin[34,35]. A dialysis device known as CritLine, an FDA approved gold standard measurement for hematocrit, was previously used to calibrate the algorithm. EE_0 and IE_0 were determined as the initial elastic and inelastic scattering acquired during the first Raman scan of an experiment.

To obtain a better understanding of the hematocrit of the spinal cord after surgery, the laser was scanned across both spinal cord and surrounding tissue to create a map of hematocrit in the area. No two points are scanned twice to avoid overlap and artificially increasing the amount of signal detected. Additionally, only muscle, bone and spinal cord were ever scanned, precluding fat and skin.

2.6 Raman Device and Post-Processing

The spectroscopic measurements employed a modified commercial Raman spectrometer (Lambda Solutions, Waltham, MA). The rest of the optics and filtering was standard for Lambda Solutions probes but there was an additional Raman notch filter (Semrock, Rochester, NY) placed between the collimating lens and the grating to allow adjustment of the elastic signal (EE) and inelastic signal (IE) for optimum range in the hematocrit calculation. A standard Raman normal incidence probe having a focal length of 1 cm was used with an effective numerical aperture of ≈0.13 and the smallest spot size was ≈100 μm. The entire surgical field and in particular the point where light contacts the tissue was kept moist in order to prevent burning

during extended exposures. The exterior surface was contacted directly with 80 mW of continuous-wave light at 830 nm.

Raw spectra were cropped to the fingerprint region of organic molecules (400 cm^{-1} to 2400 cm^{-1}) to visualize changes in the spinal cord. To remove additional noise and accentuate Raman peaks, a '101-7' arbitrary baseline correction was applied to each Raman spectra. A 101-point adjacent average of the raw spectra was obtained and subsequently subtracted from the original dataset. In addition, a 7-point average smoothing is applied to remove any excess high frequency noise inherent in the sample. The result can be seen in Figure 3, where Figure 3B shows differences in relative peak height across all time scans.

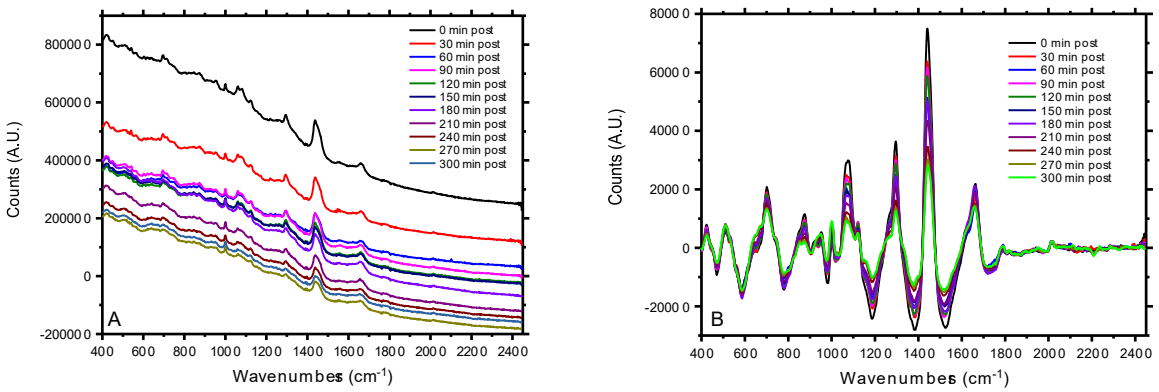

Figure 3: Example of Raman signal post-processing. A). Raw Raman spectra of scans for position A on an injured animal. Note the decrease in signal over time that can be attributed to fluorescence of the spinal cord. B). Raman data after 101-7 smoothing and dark current subtraction.

2.7 Spectroscopy Data Analysis

In order to compare peaks among samples, a baseline sample was needed to account for animal specific changes and surgical trauma in the spinal cord. For all experiments, an initial Raman scan was acquired prior to injury to serve as a 'pre-injury' internal control. All subsequent spectra and peaks were analyzed by subtracting the pre-injury spectrum from each timepoint spectrum. Peak analysis was performed both qualitatively and quantitatively based on

peak area. Relevant peaks were determined based on relative visual changes seen among spectra as well as peaks identified in literature. Peak area was determined by a change in inflection; when one curve reached an inflection point from the previous peak, this point was considered the beginning of the curve for the area. Through this method, each of the positions on the spinal cord and each experimental group were analyzed separately. Specific wavenumbers were chosen as representative peak area assignments.

To determine full group comparison from injured to uninjured, Principle Component Analysis (PCA) was performed on both datasets. PCA is a method in which correlated variables are orthogonally transformed to create a new set of variables based on the variance of the data. These new variables, known as Principle Components, can be used to reduce the dimensionality of larger datasets by combining similar variables together and is a common method of both visualizing and analyzing Raman spectra in literature[36–38]. Due to the size of the dataset, single value decomposition (SVD) was used. This is a common method of determining principal components of non-symmetric matrices. SVD uses a rectangular matrix, defined here as $A_{n \times p}$ where *n* is the number of rows and *p* is the number of columns, and through Single Value Decomposition theorem states that:

4. $A_{nxp} = U_{nxn} S_{nxp} V^T{}_{pxp}$

where U^TU and V^TV are orthogonal matrices, the columns of U are left singular vectors, S corresponds to the same dimensions as A and contains the single values along its diagonal, and V^T contains the rows that are right singular vectors corresponding to U. To determine the SVD, both eigenvalues and eigenvectors are needed from AA^T and A^TA; the columns of AA^T correspond to the columns of U and the columns of A^TA correspond to the columns of V. For the

single values in S, these values are composed of either AA^T or A^TA eigenvalues returned as square root values. From SVD theory, the matrix S can be equated as shown in equation 5.

5. $AV = USV^TV = US$

Eigenvalues and eigenvectors determined by using the covariance matrix of A are used to form the various components of the PCA. Equation 6 shows the covariance matrix definition of a symmetric matrix, but since the matrix used is non-symmetric, the definition of A is substituted from equation 4 to produce equation 7:

6. $C = \frac{A^TA}{(n-1)}$

7. $C = \frac{VSU^TUSV^T}{n-1} = V\left(\frac{S^2}{n-1}\right)V^T$

Where C is the covariance matrix for matrix A [39,40]. Given that we have the solution to matrix S, V and V^T, it is possible to solve for the covariance matrix. For this work, 3 principle components were chosen to describe nearly 100% of the variance in the data.

2.8 Statistical Analysis

Statistical analysis was performed using R studio (version 1.1.383, October 9th 2017). Comparison between peak area for both subtraction spectra and PCA peak area was performed using one factor ANOVA and unpaired Student's t-test respectively. PCA was performed using the prcomp function built in R with additional analysis using the built in R library, factoextra, corrplot, and FactoMineR extensions. Contributions of the variables to the principal components was determined using one factor ANOVA. Unless otherwise stated, all test significance was set at $p<0.05$.

Chapter 3: Results

3.1 Verification of Real-Time Raman use on Spinal Cord

In vivo Raman spectra were successfully acquired using live Raman spectra methods. To verify Raman acquisition was based on spinal cord tissue and not surrounding tissue, samples were compared to previous work performed in the lab as shown in Figure 4. Representative spectra for this study are shown in Figure 4a, Figure 4b shows spectra acquired from organotypic slice cultures of mouse spinal cords. Despite differences in preparation and scanning location, similarities across both graphs can be seen. Peak numbers of approximately 1445cm^{-1}, 1300 cm^{-1}, 950 cm^{-1}, and 700 cm^{-1} can be compared across all samples; where additional peaks not present are due to differences in white and grey matter spectra[33].

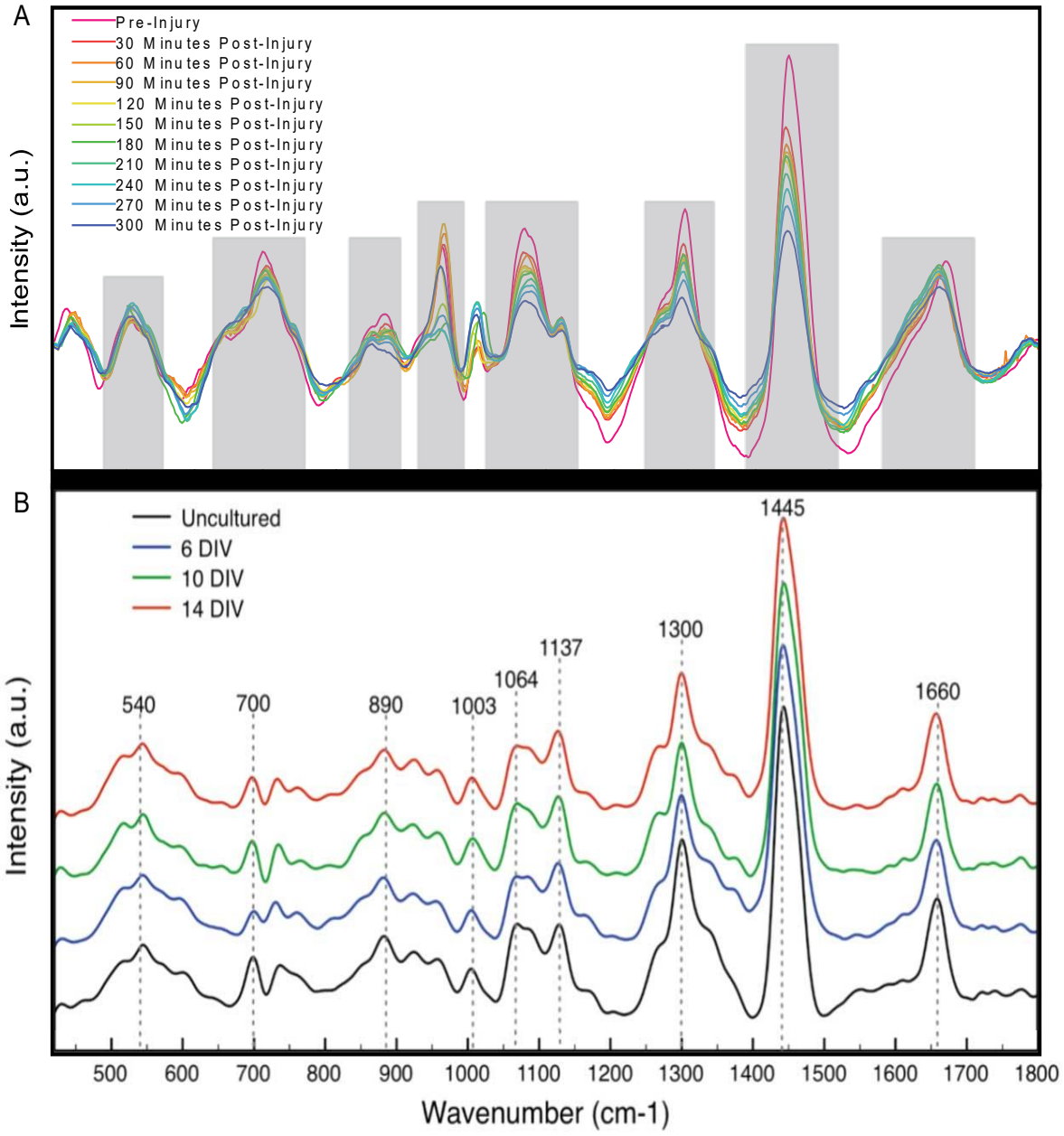

Figure 4. Graphic depiction of Raman spectroscopy for spinal cord from various sources. A). Representative sample taken from current work. Grey lines are indicative of peaks that either correlate with the other sources or peaks that are unique. Data truncated to 1800 cm^{-1} to visualize spectrum compared to other graphs. See table 1 for peak assignments and values. B). Previous lab Raman data depicting peaks obtained from organotypic slices of artificial cerebrospinal fluid infused tissue. Images were taken perpendicular to dorsal section of spinal cord compared to other graphs. Graph B shows comparable peaks compared to graph A. Graphs B was modified from source 25.

Directly after surgery, redness could be seen on the spinal cord attributed to irritation from removal of dorsal section of the vertebral column, however this discoloration receded in both controls and injury samples before initial Raman scans. During surgery, no significant changes were observed in spinal cord morphology due to Raman laser exposure or exposure to environmental conditions. Occasional hiccups from animals did cause some small perturbations in Raman acquisition that were removed prior to final Raman spectra plotting. These hiccups were believed to be simple autonomous reactions due to the anesthesia and were considered inconsequential. Fluid buildup was apparent in both control and injury samples from an unknown source; however, no change in the Raman signal or any signs of detrimental effects on the surrounding tissue were observed and the fluid was believed to be residual saline. After surgery, exposed spinal cords were lightly cleaned of excess fluids with sterile tissue paper.

3.2 Assignment of Raman Peak Values

Raman spectra bands were acquired and processed as previously described. Peak wavenumbers were assigned to represent a range as shown in the grey boxes from Figure 4A. Peak definition was determined based on previous work performed in the lab as well as areas in which changes were apparent from first scans to last. Peak area was determined by comparing inflection points in the data where curves would intersect to allow unbiased peak ranges. This enabled more focused definition of wavenumber ranges and the ability to obtain quantitative values for peak area reliably. Peak assignments can be seen in Table 1. Biochemical group assignments were based on Raman sources to biochemical markers relevant to spinal cord tissue.

Peak Wavenumber (cm^{-1})	Biochemical Assignment	Reference Number
426	Cholesterol, Serine	41
581	Phosphatidylinositol	41
662	Bicarbonate, Tyrosine	41–44
873	saccharide (β)	29,41
953	Phosphorylation	45
989	Phenylalanine	33,46
1072	Lipids	46,47
1189	Lipids	46,47
1298	Amide III	33,41
1385	Nucleotides	32,46
1439	Lipids	32,41,46,47
1666	Amide I	5,29,32

Table 1: Peak position and assignments of Raman spectra from in vivo spinal cord measurements from 400 cm^{-1} to 2400 cm^{-1}. Reference numbers refer to the biochemical assignment source.

3.3 Change of Raman Spectra Over Time

In order to obtain quantifiable changes over time, a subtraction spectrum was acquired in each of the tests performed. Subtraction spectra are determined by subtracting each subsequent Raman spectra in a single position from the first scan performed. In this case, the first spectrum of each subtraction is before the contusion injury for the injured animal cases to create an animal specific baseline.

To determine proof of concept that Raman spectroscopy can detect changes over time in in vivo spinal cord tissue, a comparison of control subtraction spectra and injury subtraction spectra of each timepoint was performed. Subtraction spectrum of each animal for all timepoints and locations were created to verify if these changes were consistent among both control and injured animals. Using the methods described above, two graphs can be seen in Figure 5 of differences occurring over the time course of the scan, with the top graph in Figure 5

representing unaltered Raman data and the bottom graph representing subtraction spectra of the same data. Qualitatively, the majority of peaks obtained in the subtraction spectrum are not the same as the initial scan with peaks tending further from zero, the point at which a spectrum would match the pre-injury scan, as time increased. Representative samples of each spectra can be seen in Figure 6 for injury and Figure 7 for control. Like the results shown previously, the injury animal shows changes away from zero in spectra at all positions with a pattern tending toward larger peaks over time. In control samples a likewise effect can be seen, however, initial scans appear to remain closer to zero than in injury scans and changes become more pronounced over time. The later timepoint spectra could be attributed to environmental factors and trauma due to surgery but were not examined in this study, however the lack of early peak changes that are present in the injured animals a possible change due to the contusion injury.

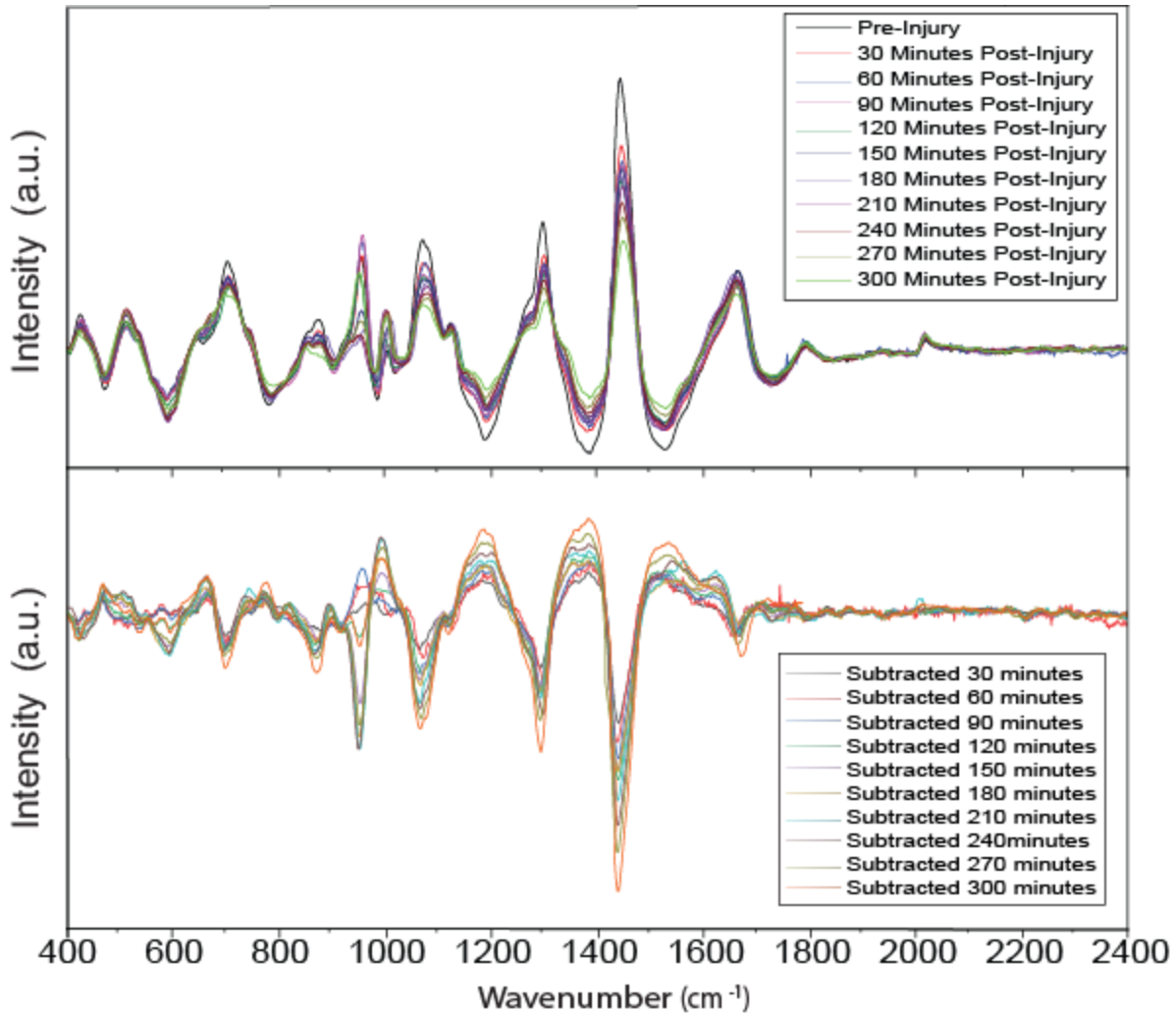

Figure 5: Representative image showing changes in spinal cord over time. Top graph shows Raman spectrum of injured spinal cord over 5-hour scan. Bottom graph shows subtraction spectra from top graph pre-injury spectra. Note that the final timepoint is the greatest change in many peaks but that is not true of all the peaks showing changes occurring throughout the procedure.

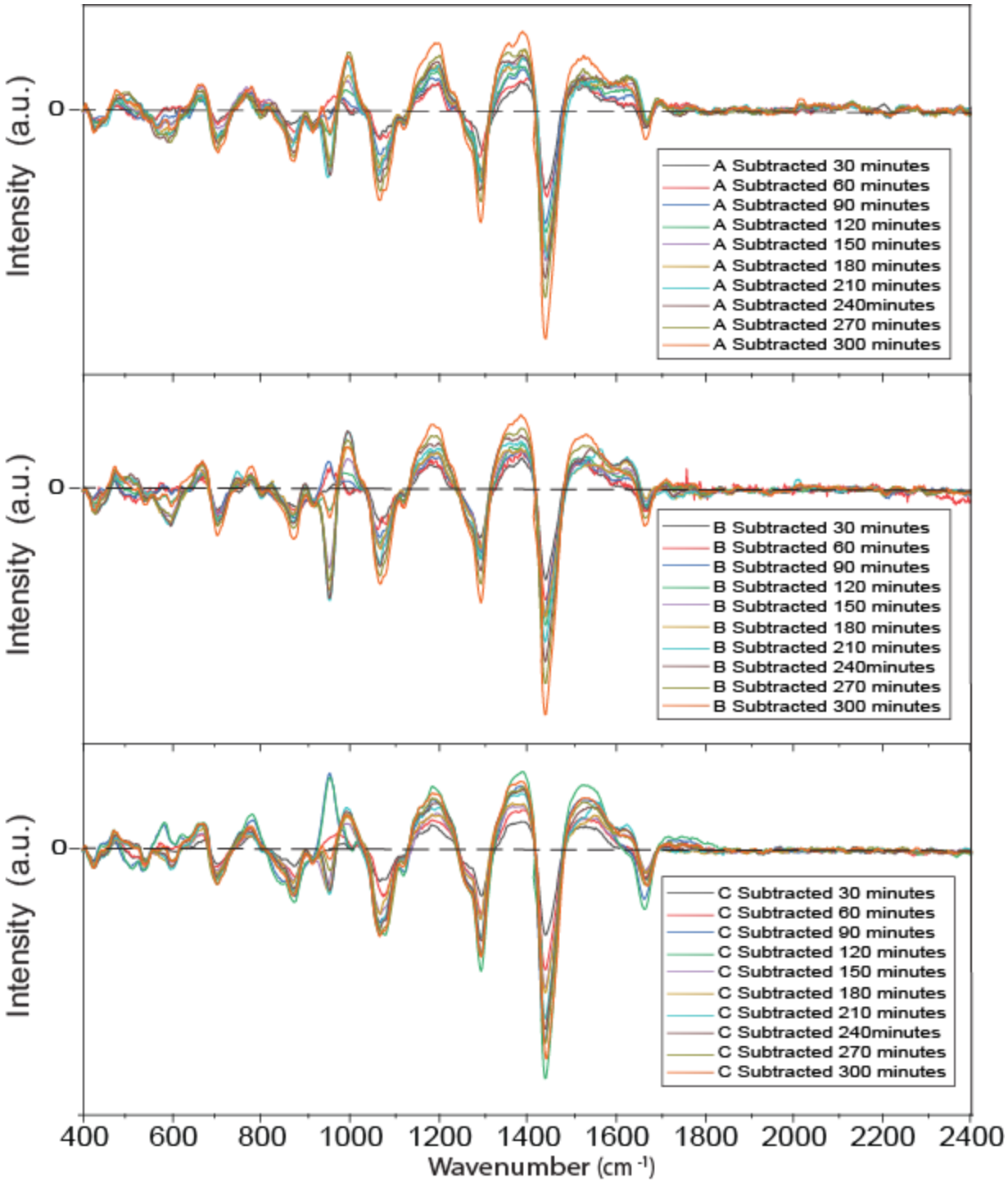

Figure 6: Representative image showing changes in spinal cord of injury using subtraction spectra with respect to each position on the spinal cord. Spectra are acquired by subtracting each timepoint spectra from the pre-injury spectra acquired before contusion injury. Dotted black line is representative of zero, where values on that line show no difference from the pre-injury spectrum, indicating no change over time. Qualitatively, all peak wavenumbers from table 1 change with respect to the initial scan for all positions.

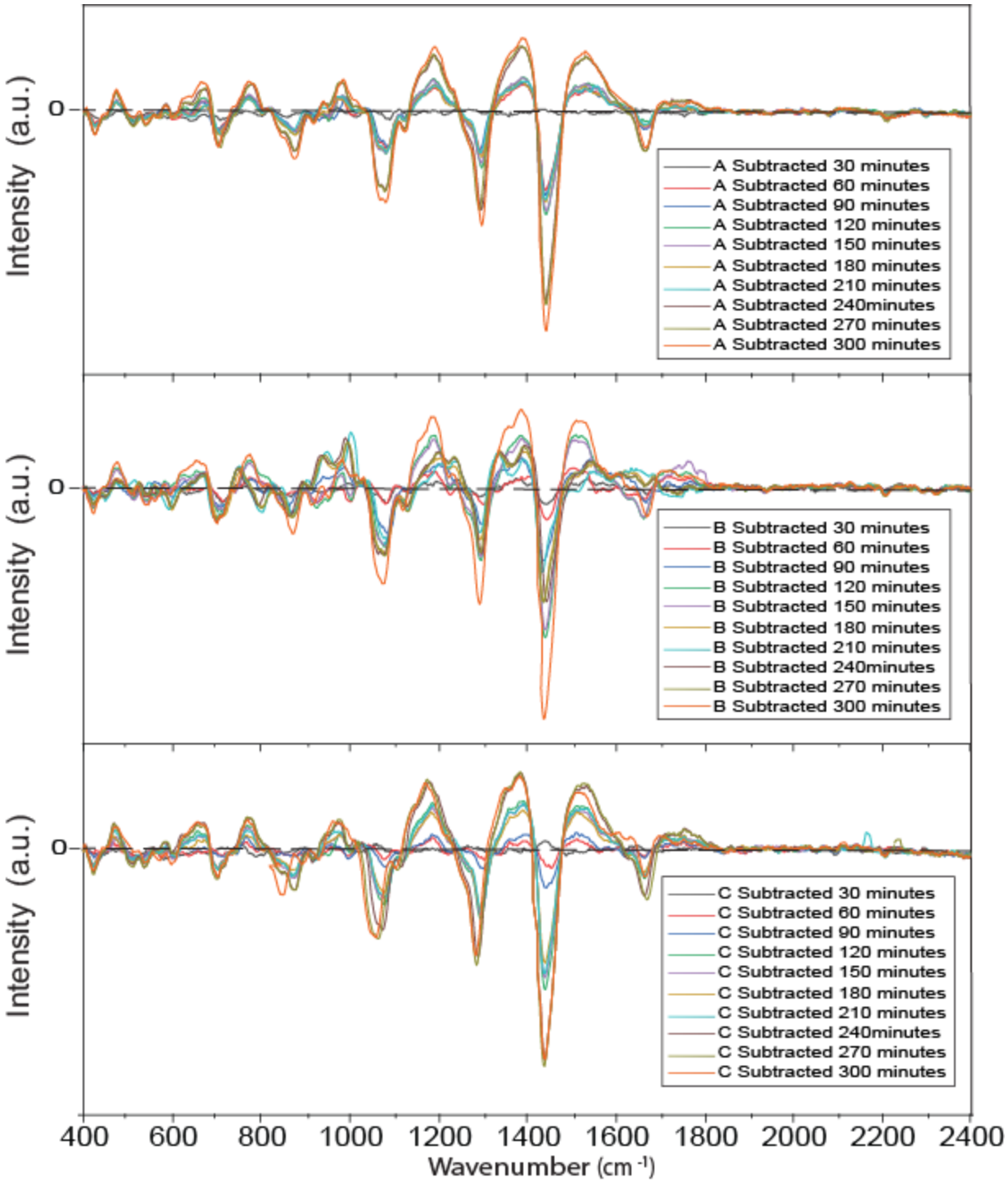

Figure 7: Representative image showing changes in spinal cord of control animals using subtraction spectra with respect to each position on the spinal cord. Dotted black line is representative of zero, where values on that line show no difference from the pre-injury spectrum, indicating no change over time. Qualitatively, for all 3 positions, the 30 minute timepoint denoted by the solid black line is closest to the dotted line, with subsequent timepoint curves changing similar to Figure 5.

To quantify the differences, the peak area under each timepoint curve was calculated, an average was determined, and ANOVA was performed comparing injury subtraction spectra to control subtraction spectra; significance comparing peak area for multiple wavenumbers is shown in Table 2. Position A shows significance at both the bicarbonate and Amide I wavenumbers, while position C shows significance at C-C lipid bending, indicating the possibility that an increase in bicarbonate and a decrease in protein formation is occurring towards the rostral end of the animal while a possible increase in lipid formation is occurring towards the caudal end. Position B shows a greater degree of significance across multiple wavenumbers indicating possible cell infiltration into the area (DNA), decrease in protein formation (Amide I and III), an increase in lipid formation (C-C lipid bending) and an increase in tyrosine concentration likely indicative of regulating ion channels after injury[6,29,48]. The greater degree of significance in position B is highly indicative of changes due to the contusion injury, showing that changes in response to the injury can be successfully acquired using Raman spectroscopy technique; however, the high similarity of peak change over time in control animals compared to injury indicate that either environmental effects, the surgical procedure, or the Raman laser itself may be causing unknown injury to the tissue compared to healthy cord.

Differences between Control and Injury Area p-values					
Peak (cm^{-1})	Assignment	Change	Position A	Position B	Position C
426	Serine	⬆	0.17	0.38	0.41
662	Bicarbonate, Tyrosine	⬆	0.016	0.20	0.40
1072	C-C Lipid Bending	⬆	0.94	0.045	0.045
1189	Lipid	⬆	0.85	0.050	0.43
1298	Amide III	⬇	0.96	0.045	0.44
1385	DNA	⬆	0.95	0.050	0.42
1439	CH2 Lipid Bending	⬇	0.88	0.060	0.41
1666	Amide I	⬇	0.010	0.012	0.48
Legend:				p>0.05	0.05≥p

Table 2: Comparison of subtraction peak area wavenumbers between control and injury animals. Significance is determined at p<0.05 and was performed by ANOVA. Red coloring indicates non-significance of a wavenumber at a position. The majority of significance is found at position B, at the site of injury, while few wavenumbers at positions A and C show differences.

3.4 Principle Component Analysis

Principle Component Analysis (PCA) was performed to further examine the effect time has on changes in the spinal cord and to observe possible changes that may be occurring between injury and control animals as shown in Figures 5 and 6. Due to the quantity of variables and high similarity among the timepoint scans, data was compiled into two sets of injury and control for each n=3 to observe variance of each position across all timepoints. Raman spectrum data was used from 400 cm^{-1} to 2400 cm^{-1}.

To capture greater than 99% of the variance in the data, three components were created for both control and injury data. Representative graphs of the averaged principal component analysis loading for both groups are shown in Figures 8-10. Loading graphs are measures of the importance of a wavenumber on the original data, with greater magnitudes indicating greater influence. Each position was compared between the two groups and peak area was calculated

using student t-tests at $p<0.05$. Significance results are shown in Table 3 for each position and component. For component 1, much of the variation in the data closely follows that of the normal Raman spectrum for both injury and controls. Significant variations in the peak areas of position C can be seen, but only a single instance of significance at 662 cm^{-1} is shown at position A and no significance can be seen at position B. 662 cm^{-1} for position A is attributed to tyrosine in this case that also shows a Raman peak in spinal cord tissue at this wavenumber[41,46]. For position C, 581 cm^{-1} is indicative of phosphatidylinositol, a lipid present in spinal cord tissue, while 1072 cm^{-1}, 1189 cm^{-1}, 1385 cm^{-1}, 1439 cm^{-1} and 1666 cm^{-1} are represented as described previously in Table 1.

Component 2 shown in Figure 9 shows large changes in injury compared to control animals among many peak areas. 1072 cm^{-1}, 1189 cm^{-1}, 1298 cm^{-1}, 1385 cm^{-1}, 1439 cm^{-1} are likely indicative of lipids, DNA and protein concentration changing due to increased cell migration to the injured cord[6]. Unlike previously in component 1, the double peak indicated by 662 cm^{-1} is attributed to bicarbonate ions due to their well-known peak profile and relatively high concentration in spinal cord cerebrospinal fluid[44,49]. The 873 cm^{-1} peak shows change in saccharides while the 953 cm^{-1} peak is a possible indicator of phosphorylation of proteins[33,45,48]. While position B only shows significance at 662 cm^{-1} and 953 cm^{-1}, many of the other wavenumbers show near significance; position A shows similar near significance at many of the shorter length wavenumbers. Position C shows high similarity to the previous component, with levels of significance across a majority of the wavenumber peaks.

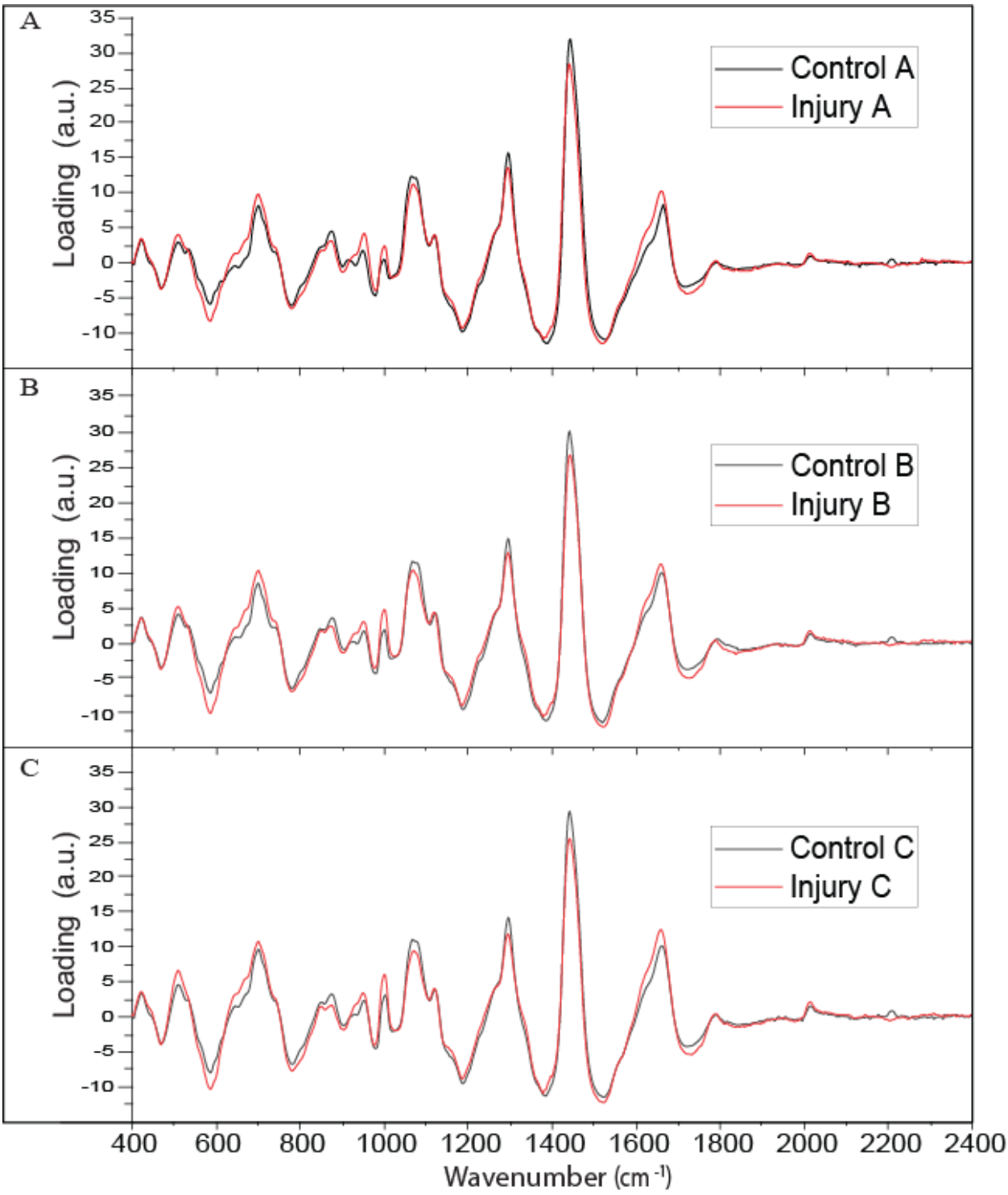

Figure 8: Graphs depicting the first principal component at each position for both injury and controls. A). Principal component 1 for position A. B.) Principal component 1 for position B. C.) Principal component 1 for position C. While all graphs qualitatively show high similarity between injury and control, changes in peak amplitude at multiple wavenumbers can be seen.

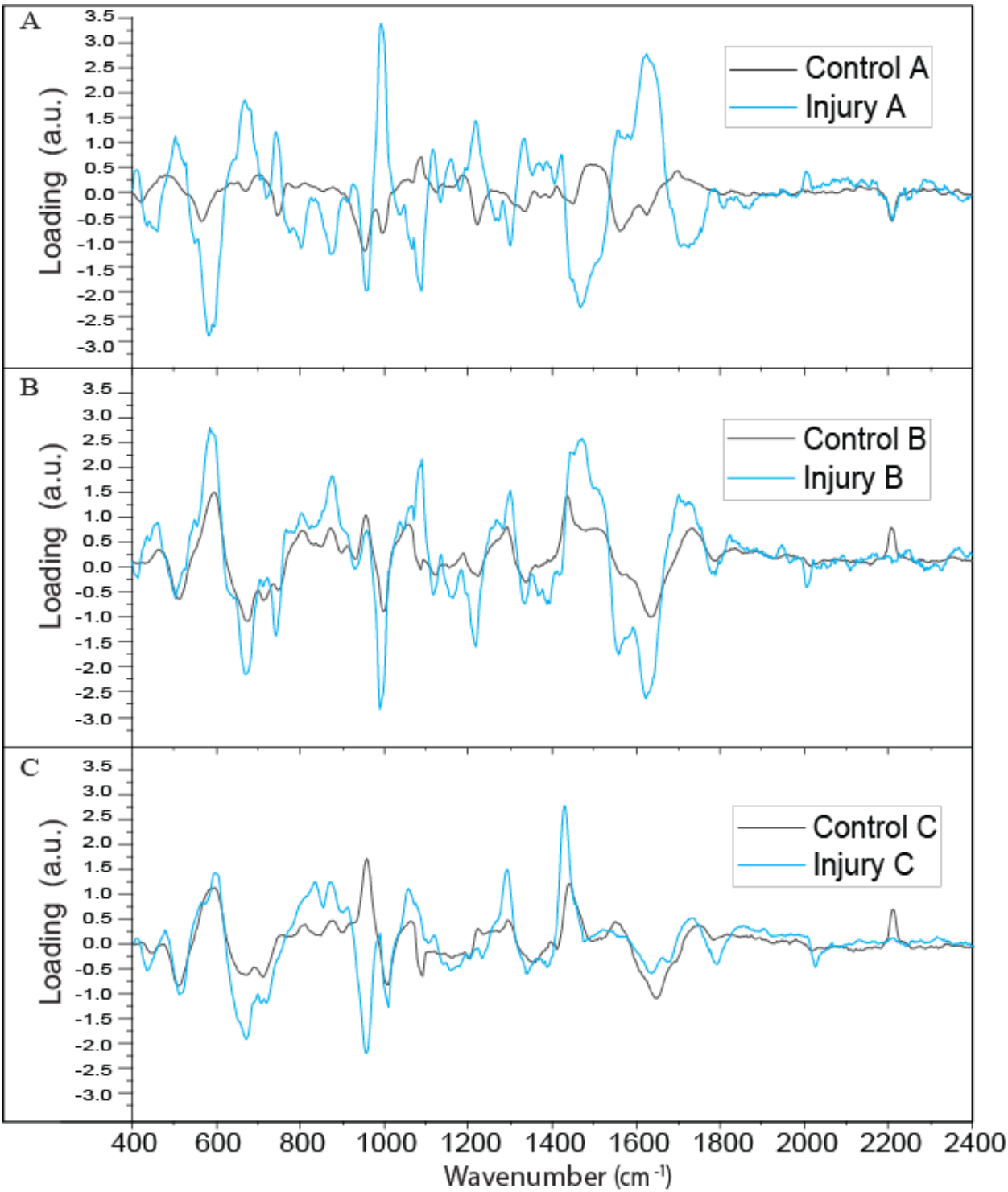

Figure 9: Graphs depicting the second principal component at each position for both injury and controls. A). Principal component 2 for position A. B.) Principal component 2 for position B. C.) Principal component 2 for position C. Large fluctuations in peak loading amplitudes can be seen throughout all positions. This is primarily due to a single injury animal affecting the loading curves, however, significant results can still be seen as shown in table 3.

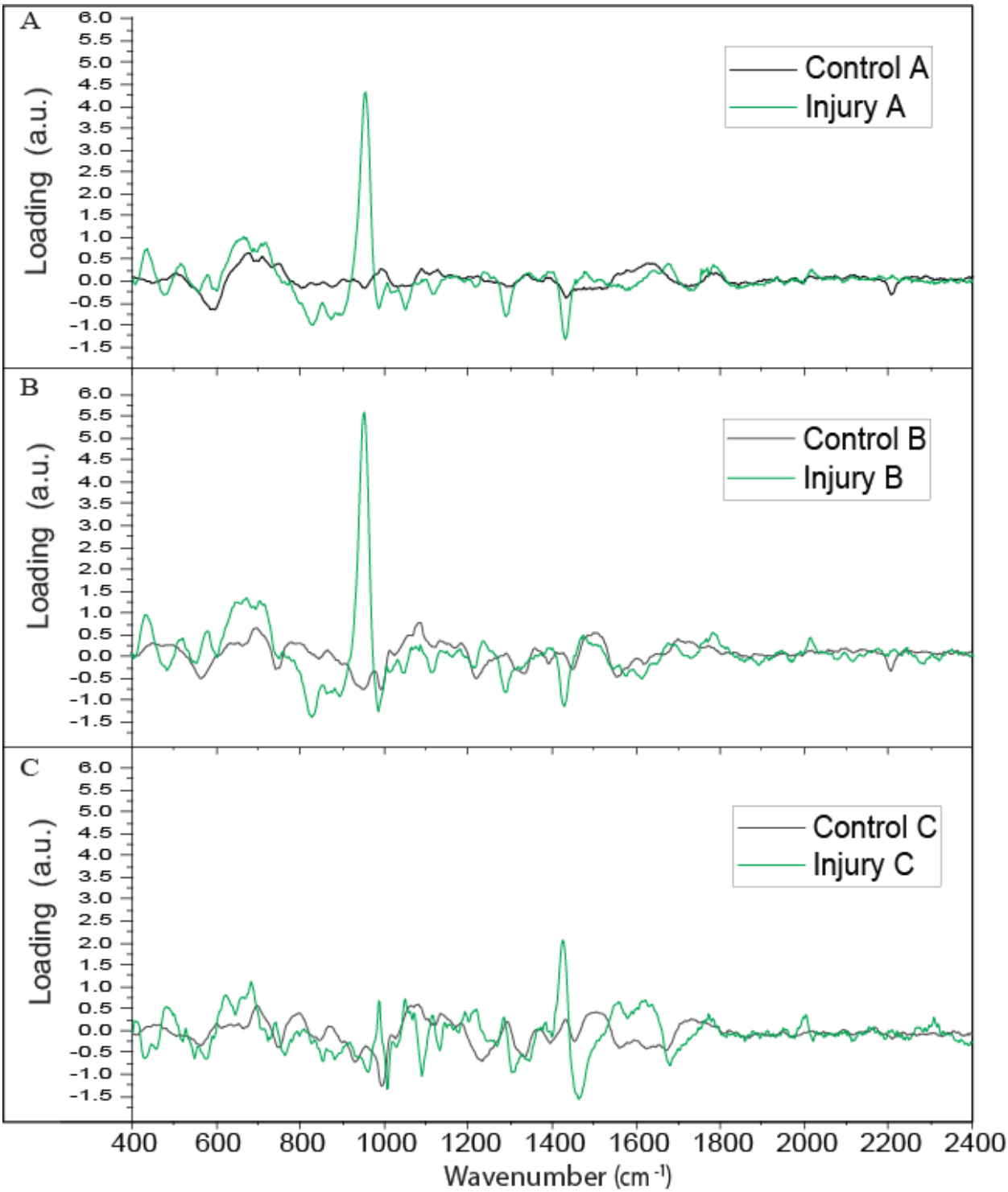

Figure 10: Graphs depicting the third principal component at each position for both injury and controls. A). Principal component 3 for position A. B.) Principal component 3 for position B. C.) Principal component 3 for position C. Graphs A and B injury curves show specific peaks at 953 cm^{-1}, and 1439 cm^{-1}. Graph C shows greatly reduced peak amplitude for the injury curve compared to positions A and B.

Principal Component Analysis Table of Peak Area Significance between Injury and Control									
	Component 1			Component 2			Component 3		
Wavenumber (cm^{-1})	Position A	Position B	Position C	Position A	Position B	Position C	Position A	Position B	Position C
426	0.76	0.96	0.55	0.022	0.092	0.031	0.79	0.22	0.19
581	0.18	0.088	0.034	0.072	0.10	0.059	0.85	0.94	0.80
662	0.042	0.21	0.18	0.068	0.050	0.014	0.70	0.21	0.70
873	0.16	0.16	0.075	0.064	0.063	0.046	0.12	0.24	0.30
953	0.45	0.61	0.56	0.021	0.050	0.024	0.0065	0.036	0.36
989	0.33	0.17	0.050	0.10	0.057	0.337	0.39	0.55	0.057
1072	0.22	0.13	0.0049	0.10	0.062	0.033	0.25	0.57	0.024
1189	0.35	0.24	0.0073	0.16	0.098	0.031	0.74	0.33	0.22
1298	0.14	0.27	0.12	0.14	0.070	0.010	0.049	0.24	0.45
1385	0.17	0.13	0.018	0.12	0.12	0.034	0.12	0.37	0.17
1439	0.16	0.10	0.022	0.095	0.068	0.049	0.027	0.075	0.038
1666	0.27	0.18	0.039	0.087	0.058	0.072	0.31	0.94	0.0048
Legend:								p>0.05	0.05≥p

Table 3: Peak area comparison between injured and control principal component analysis wavenumber loadings among all positions. Significance was determined at p>0.05 and areas were compared by unpaired student t-tests. Green colored cells indicate significance while red colored cells indicate a lack of significance.

Component 3 shows an increase in injury curves at three peaks at for position A: 953 cm^{-1}, 1298 cm^{-1}, and 1439 cm^{-1}. The 953 cm^{-1} peak is attributed to additional phosphorylated proteins caused by the injury and is also present at position B. The presence of both 1298 cm^{-1} and 1439 cm^{-1} peak structures are suggestive of additional amide I and lipid formation. Position C shows lower magnitude peaks at 953 cm^{-1} while maintaining a peak at 1439 cm^{-1}, however the 1298 cm^{-1} peak is no longer significant, and an additional significance is found at 1666 cm^{-1} indicative of amide III.

Based on the orthogonal nature of each principal component, the results can be depicted as describing altogether different compositions within the spinal cord based on each component. The high similarity of the first component wavenumber amplitudes to those of the original data suggest that the first component is likely depicting static tissue. The amount of variance depicted, ~ 95%, in the first component also explains this as the majority of the spinal cord being measured would be tissue. The second component is believed to be cerebrospinal fluid. The presence of the double peak in the data shown at 662 cm^{-1} indicative of bicarbonate is explained by the high concentration of bicarbonate in spinal fluid[44,50]. Additionally, the presence of

phosphorylation could also be explained by the presence of Tau proteins found in cerebrospinal fluid after injury[50]. The third component is likely explained by plasma; however, a relatively low amount of variance, less than ~1%, shows a high volume of noise compared to the other two components, making the exact composition difficult to discern.

Due to the location of position C caudal to the injury site, it is likely that the extent of swelling was reduced compared to the rostral position, A, and the injury site, B. Previous work performed in rats at T10 showed that compression caused decreased blood flow of the injury and surrounding area and ischemia tended to expand into the rostral end greater than the caudal end[51]. This is likely the cause of decreased significance throughout components A and B due to a change in focal spot of the Raman laser from swelling of the tissue. Wavenumbers at 662 cm^{-1}, 953 cm^{-1}, 1072 cm^{-1}, 1189 cm^{-1}, 1385 cm^{-1}, and 1439 cm^{-1} are the most common peaks to show significance among components and positions. 953 cm^{-1} indicates high levels of phosphorylation among injury models compared to controls at all positions. 662 cm^{-1} shows decreased levels of tyrosine in component 1 for position A, while its change in component 2 is indicative of levels of bicarbonate ions in the injured area, likely originating from cerebrospinal fluid to regulate pH balance and astrocyte swelling in the area due to ischemia[17,44,49,52]. Significance of lipids in injury could be attributed to swelling of the surgical area. The Raman laser being used is fixed in position before the experiment begins; as swelling of the tissue occurs due to the inflammation response the amount of tissue being measured may change as mentioned previously. Primarily, the Raman signals represent white matter, the tissue in the central nervous system (CNS) rich with lipid content, due to penetration of the laser. Changes in measurement of lipids can be expected in position C due to little change in focal position affecting the amount of white matter being measured; as is seen at 1072 cm^{-1}, 1189 cm^{-1}, and 1439 cm^{-1} [33]. Positions A and B are

likely not measuring as many differences due to the focus of the laser changing. Amide I and III, denoted by 1666 cm^{-1} and 1298 cm^{-1} respectively, are well known vibrational bands corresponding to protein content in a sample. The presence and increase of these peaks indicates production of proteins, such as myelin and lymphocyte protein (MAL) and tau protein, that are known to increase during spinal cord injury[33,53,54].

3.5 Analysis of Timeline for Injury

Principal component analysis was also performed on each individual animal to visualize any trends that time may have during injury. The percent contribution of a timepoint to a component was used for both injury and control animals. Cosine squared values of the variance for each timepoint were used and percentages were calculated by dividing by the total variance to obtain percentage values. ANOVA was used to determine significance of a contribution to the sample; in all situations, values greater than 10% contribution were significant. A representation of the division of contributions for a sample can be seen in Figure 11, where the dotted red line indicates the 10% contribution limit. Values greater than this were counted for both injury and control animals at each position and the results can be seen in Tables 4 and 5 for cerebrospinal fluid and plasma respectively. Static tissue was not included as all timepoints showed equal contribution, resulting in no significant difference.

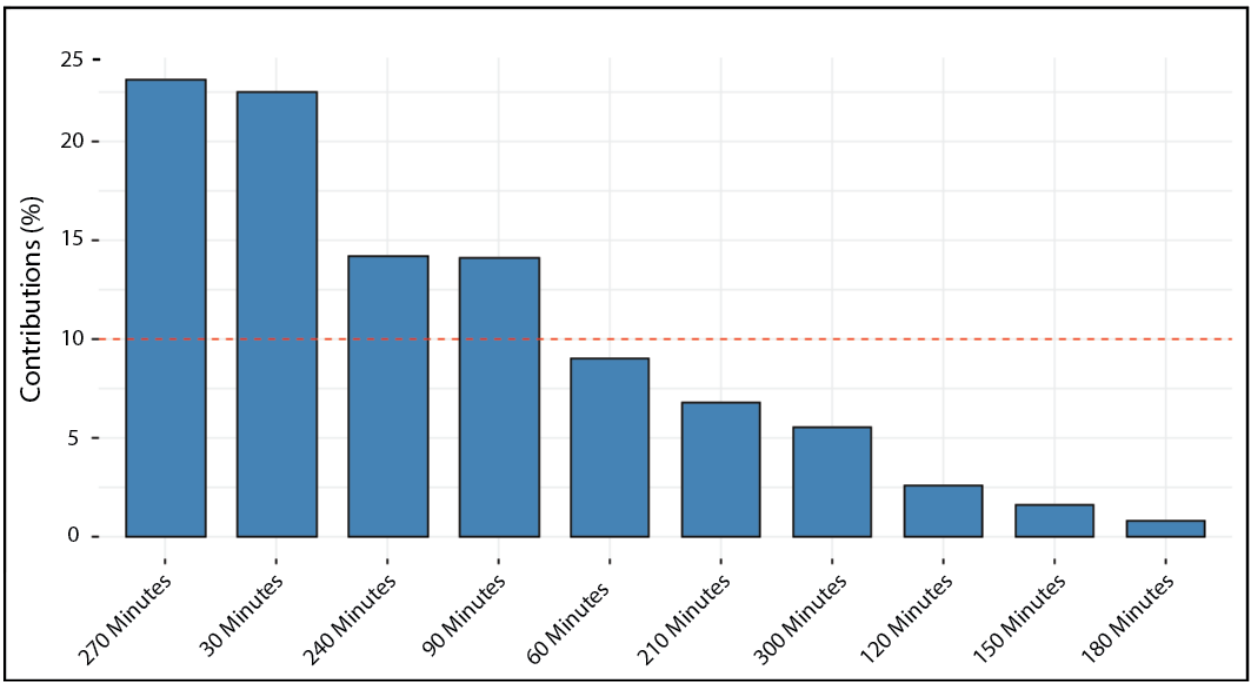

Figure 11: Representative graph depicting contributions of individual timepoints to an animal. Red dotted line indicates the 10% contribution level. Values greater than this were used to determine a trend in timepoint data for injury and control animals.

Table 4 shows a tendency for injury timepoints to have significant contributions from 30 minutes to 90 minutes and from 240 minutes to 300 minutes at all positions, while controls show a more randomized pattern including timepoints such as 120 minutes and 180 minutes. Injury position C also shows contributions at 150 minutes that may be due to different effects of ischemia on the location compared to positions A and B. Table 5 shows far greater variation in timepoint contribution to plasma than compared to cerebrospinal fluid for both controls and injury animals. Though injury tends to have a greater number of animals that have significant contributions at the early, 30 minutes, and late, 300 minutes, timepoints, there are also many contributions that are shown throughout the timeline. In a similar manner, control contributions tend to show timepoints in a seemingly random pattern as before, though two animals show

Component 2 Timepoint Contributions						
Time (minutes)	**Injury A**	**Injury B**	**Injury C**	**Control A**	**Control B**	**Control C**
30	1	2	2	1	2	1
60	2	1	1	1		1
90	1	2		1	1	2
120					1	
150			2	2		1
180					1	1
210	1					
240	1	1	1	1	2	1
270	1	2	2		1	
300	2	1	2	3		

Table 4: Count of significant contributions to component 2 each measured timepoint made to injury and control for each position. Significance, p<0.05, was determined by ANOVA of the squared cosine variance for each timepoint; >10% contribution was used. Injury shows grouping near early timepoint (30-90 minutes) and late timepoint (240-300 minutes) compared to controls at all positions. Green corresponds to all three animals contributing, yellow corresponds to two animals contributing, while red corresponds to a single animal contributing for ease of visualization.

Component 3 Timepoint Contributions						
Time (minutes)	**Injury A**	**Injury B**	**Injury C**	**Control A**	**Control B**	**Control C**
30	2	2	3	2		3
60		1	1	1	2	1
90	1	2	1		1	1
120		1	1	2		2
150	1				2	
180			1	2	1	
210	2	1	1		1	2
240	2		1	1		1
270	1	1	2	3	2	1
300	2	2	1	1	2	1

Table 5: Count of significant contributions to component 3 each measured timepoint made to injury and control for each position. Significance, p<0.05, was determined by ANOVA of the squared cosine variance for each timepoint; >10% contribution was used. Injury shows some grouping near early and late timepoints compared to controls, but a greater distribution of contributions at timepoints not seen in Table 4. Green corresponds to all three animals contributing, yellow corresponds to two animals contributing, while red corresponds to a single animal contributing for ease of visualization.

significant contributions often in the time period of 120 minutes to 210 minutes compared to injury contributions.

Though no significant conclusion can be made from this, trends do show that early and later timepoint contributions tend to affect the data greater than interim timepoints in injury

animals for all positions compared to controls. Injury cerebrospinal fluid shows the greatest difference from 30 minutes to 90 minutes and from 240 minutes to 300 minutes, while injury plasma also shows similar, if less pronounced, results on early and late timepoint contributions to the data; control timepoints tend to show a far more distributed contribution among the timepoints that, given the lack of substantial damage to the tissue, is expected from the lack of an immune response to injury.

3.6 Mapping of spinal cord hematocrit

Raman spectroscopy also has applications in measuring both topographical information as well as hematocrit data for live tissue samples[34,55]. A single healthy animal was used to scan the Raman probe across the cord in a pattern designed to never scan over the same location twice to avoid bleaching effects of the laser. IE and EE taken from the scan were used as previously described to obtain apparent hematocrit levels of the spinal cord shown in Figure 12. Higher concentrations of apparent hematocrit can be seen at the approximate center of the spinal cord corresponding to the anterior spinal artery and extending capillaries[56]. Lower levels of apparent hematocrit in the surrounding tissue can be attributed to distance from the Raman laser and not remaining in the field of focus. By visualizing apparent hematocrit levels in the spinal cord that correspond to known anatomy, the possibility of measuring changes in blood accumulation during injury is a future methodology that Raman spectroscopy may be capable of performing in in vivo spinal cord measurements.

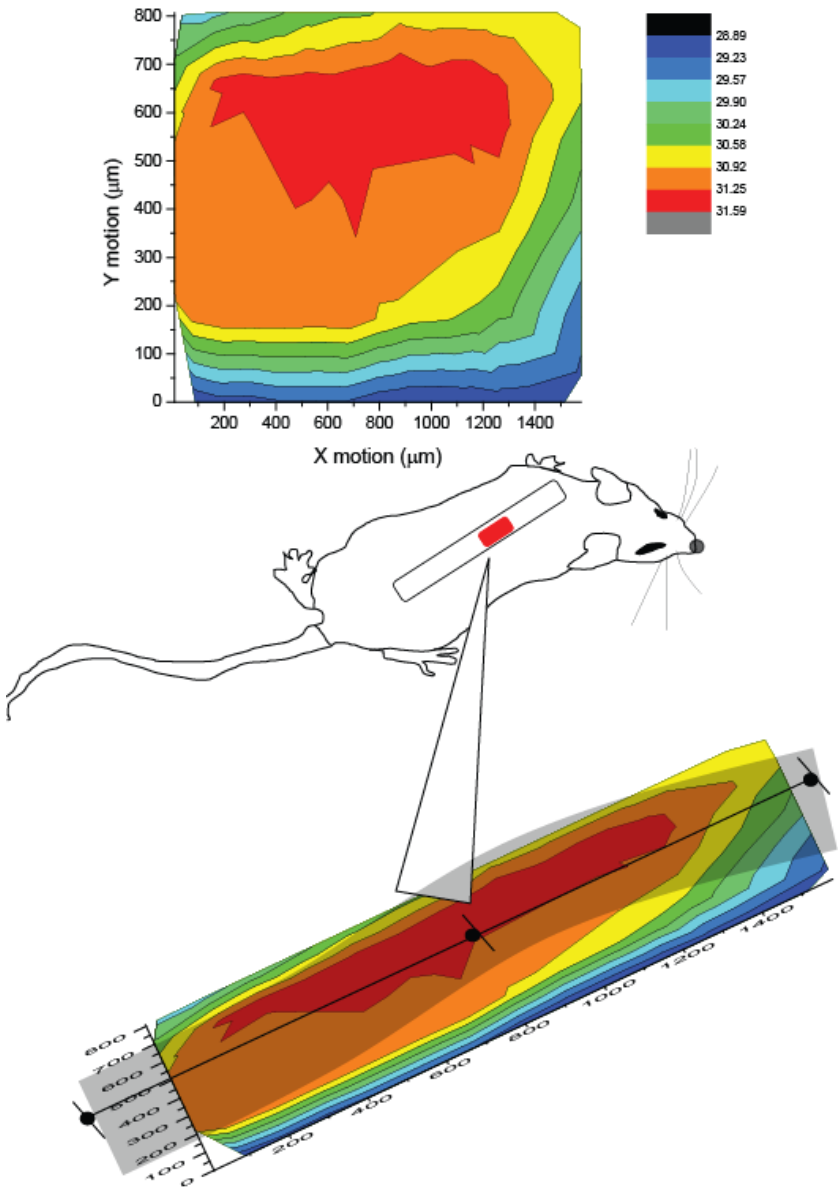

Figure 12: Image of surgical field including spinal cord of healthy subject based on apparent hematocrit values determined by PV[O]H software for calculation of blood metrics[35]. Obtained in a scan trajectory designed so that no point can get probed twice, reducing overlap. Mapping shows possible application in determining rough concentration of blood volume before and after injury.

Chapter 4: Discussion

Raman spectroscopy is a strong analytical tool for examining the highly dynamic nature of living tissue. As mentioned, previous works have used the technique in avenues such as cancer detection[23], determination of atherosclerotic plaque buildup[26], ex vivo spinal cord tissue assessment of injury[5,29], and measuring the brittleness of living bone[24]; however, to our knowledge, no work has been shown to use Raman spectroscopy to analyze changes in vivo of spinal cord injuries. This study presents a novel application of Raman spectroscopy to measure chemical and physical changes in the spinal cords of rats over time after the effects of a contusion injury to better understand the complex makeup of early SCI in vivo.

To start, we gathered multiple scans of 3 specific locations along the exposed spinal cord of female rats, one location towards the head of the animal, one in the center at the contusion drop location, and one towards the tail end of the animal as shown in Figure 2. This was done to observe any locational changes that could occur as an after effect of the contusion injury and to gather as much information about the spread of injury as possible. We show that, compared to the timepoint before injury, the location at the injury site shows the greatest amount of significant difference in the injured animals compared to controls. While this result agrees with our initial hypothesis, there were additional factors in both positions surrounding the injury site that warrant further discussion. The following will discuss the significant differences between subtraction spectra of injured and uninjured animals and the Raman assignments shown in Figures 5 and 6 and Tables 1 and 2, respectively.

At position A in the cord, we saw an increase at 662 cm^{-1} and 1666 cm^{-1} in injured animals compared to that of the uninjured controls. 1666 cm^{-1} is attributed to that of Amide I, a well-known marker of protein concentration. Its decrease could be attributed to swelling in the

area of the injured animals compared to uninjured, changing the concentration of the protein content being measured within the tissue as the Raman laser becomes unfocused. 662 cm^{-1} could be attributed to either tyrosine or bicarbonate ions in the area. Tyrosine has an identifiable peak at this point attributed to benzine ring deformation[57] while bicarbonate normally has a very distinct double peak present representative of CO_2 bending modes in the molecule[44] but due to lower concentrations compared to tyrosine, especially in injured animals, it may not be easily visible[50,58]. The presence of significance in only position A for 662 cm^{-1} agrees with previously reported work previously that described swelling of tissue increasing further toward the head of the animal compared to that of the tail. As the swelling increases, tyrosine, a precursor to epinephrine and other essential neurotransmitters[58], may be in higher concentrations than that of other locations in the cord around the injury. This hypothesis requires further testing.

At position B, many of the significantly different wavenumbers correlate with previous findings on spinal cord injury. Previous work performed in our lab[29] showed significant changes at 1666 cm^{-1}, 1385 cm^{-1}, 1189 cm^{-1}, and 1072 cm^{-1} corresponding to the results shown in this work. Interestingly, 1298 cm^{-1} was investigated previously, but did not show significant changes 4 days after injury; this result could be due in part to the length of time being measured or the type of injury, hemi-section incision compared to contusion, being performed[5]. The presence of lower concentrations of amide I and amide III, 1298 cm^{-1} and 1666 cm^{-1} respectively, may be an indication of reduced protein concentration in the injury area similar to the previous instance at position A. Increases in 1385 cm^{-1} are likely due to increased cell infiltration into the injured site as part of the wound response. The increases at 1189 cm^{-1} and 1072 cm^{-1} are attributed to lipid content in the sample. Previously, lipid content was shown to decrease in relation to demyelination at the injury site after SCI due to the high lipid content of myelin[29], however its

increase may be due to cell infiltration similar to increases in DNA concentration at 1385 cm^{-1}. Position C shows only one instance of significant difference from injured to uninjured animals at 1072 cm^{-1}. This difference may be due to lipid concentration. The lack of additional significant lipid peaks at any other wavenumber make this result likely to be that of cholesterol concentration[47].

Overall the changes in the spinal cord measured by Raman spectra show similar bands to those previously reported in literature[5,29], though differences in methods warrant further discussion. One major observation in using live, in vivo Raman spectroscopy is the high similarity in intensity between that of the control spectra and injured spectra. Control spectra show a determinedly monotonic increase over time at each position compared to that of the injured spectra that show increases, but not to the same extent. A possible result of doing live experiments may be that the Raman laser itself is causing damage to the tissue over time, resulting in the changes seen. Additionally, exposure to an open environment and subsequent use of anesthesia may also be affecting results. While these factors were not accounted for, it was still observed that changes at the injury site and in nearby locations could be determined, indicating that Raman spectroscopy can be used as a method to determine changes in rat spinal cords in vivo as a result of contusion spinal cord injury.

Principal component analysis was performed to measure changes in the cord that were not seen with the subtraction spectra analysis. Principal components can be used to segregate the data into separate orthogonal components that can be characterized into different aspects of the spinal cord composition. In our case, we chose the first principal component to symbolize static tissue, the second component to symbolize cerebrospinal fluid, and the third component to

symbolize plasma based on the percent composition of each component and general physiology of the spinal cord.

Static tissue shows a high similarity to the original spectra for both the control and injury spectrum at each location. This helped to choose static tissue as the primary source for this component. In comparing injured to control spectra as seen in Table 3, both position A and position B show little significant change from control to injured spectra, however, position C shows many significant wavenumbers. This change may be caused by blood flow from the rostral to caudal areas. Previous work performed by Farrar et. al. showed that blood flow along the dorsal half of the spinal cord flows from the head of the animal towards the tail while at interspaced locations throughout, additional flow is seen radially along the spinal cord[59]. As injured tissue constituents flow from position A and B towards position C, additional changes in the injured spinal cords compared to control spinal cords could be observed. Additionally, due to expected reduced swelling in the area[51], laser penetration of position C compared to positions A and B is possible. The experimental procedure did not account for additional swelling in the cord at different locations, as the laser was set before injury and its height was never changed through the course of the experiment. As such, changes in the spinal cord height due to swelling were not accounted for, and the laser focal point would change over time as the spinal cord would swell. Since position C is expected to have the least amount of swelling compared to positions A and B, it is likely that changes can be attributed to both flowing constituents towards the site and appropriate laser focusing.

The second component corresponding to cerebrospinal fluid shows high levels of near significance across nearly all wavenumbers for all positions. The primary rational for choosing cerebrospinal fluid comes from the addition of a double wavenumber peak appearing in the

loading spectra at 662 cm^{-1}. This wavenumber is a very well defined peak type corresponding to bicarbonate, a compound found in high concentrations within cerebrospinal fluid[44,50]. During injury, it is also known that increases in bicarbonate levels can be seen and affect both the ion balances in neuronal function and astrocytic neurotransmitter functions[52]. The presence of a peak at 953 cm^{-1} is also taken into account, as this peak is considered to be an indicator of phosphorylation, a process commonly seen within cerebrospinal fluid occurring at serine and threonine sites on tau proteins[47,54]. In addition, the high level of near significance for most wavenumbers shown in cerebrospinal fluid at each position may indicate that a large amount of early spinal cord injury changes are occurring in the interstitial fluid between static tissue. This is logically sound, as immediately after injury, cell constituents from necrotic damage from the contusion injury will be released into the interstitial space comprised of cerebrospinal fluid. Additional ions contained in the fluid will begin to "leak" into the tissue due to damage, resulting in a complex cascade of events resulting in the secondary phase of spinal cord injury[6,50,54].

The third component we measured is attributed to plasma and additional changes not presently shown in either static tissue or cerebrospinal fluid. The primary rationale for this assignment is the expected volume of plasma in the space compared to the other two components and its contribution, as the third component, comprises less than 1% of variance in the data. This results in a high amount of noise in the data to compare, though some wavenumbers corroborate this result. Thrombin, an important enzyme used in clotting of blood through conversion of fibrinogen to fibrin, is known to have Raman spectra peaks at 1439 cm^{-1}, 1666 cm^{-1}, and 1298 cm^{-1} [60,61]. These wavenumbers all correspond to significant peaks seen in plasma, though not in every position. The lack of ubiquitous significance across the positions may be due to the high level of noise or possible presence in control animals due to the surgical procedure.

Additionally, measurement of the contributions each timepoint had in relation to cerebrospinal fluid and plasma from the principal component analysis for both injury and controls are shown in Tables 4 and 5 with static tissue omitted as the contributions from time were nearly uniform. Each of the animals measured, n=3 for injury and n=3 for control, were used and timepoints contributing at least 10% to the component were retained. This method was used to find possible trends that may be occurring in both controls or injuries with regards to when the greatest contributions to the data were being observed. For cerebrospinal fluid, there appeared to be a trend that showed clustering of the data at early timepoints, comprising 30 minutes, 60 minutes and 90 minutes, and for later timepoints, at 240 minutes, 270 minutes and 300 minutes for injury animals. Control animals did not show any specific trend, showing a more random distribution of occurrences. Due to the lack of a specific injury in control animals the non-specific grouping of timepoint contributions is a logical outcome. It needs to be mentioned, however, that for many cases only a single animal was counted at specific timepoints for a location regardless of injury or control. Despite this, future experiments can benefit from focusing on both early and late timepoints during injury specifically for confirmation that these timepoints show the greatest effects on cerebrospinal fluid change. Measurements were also performed for plasma shown in Table 5, however, no clear pattern was discerned from these results. Whether a factor of the low contribution of plasma to the data or low signal to noise ratio is unknown.

A final measurement was used to determine if Raman spectroscopy could be used to measure the apparent hematocrit of a live, in vivo rat spinal cord. IE and EE measurements were able to simulate hematocrit levels across the surgical area and could be used to represent blood concentration levels within the spinal cord[35]. As mentioned previously, the red measurement

shown in Figure 11 is attributed to the anterior spinal artery running longitudinally along the spinal cord. Measurements were acquired using a pattern that scanned the whole surgical area without scanning over a location twice to avoid oversampling. While blood may have pooled in muscle tissue surrounding the cord, a drop in hematocrit levels from the spinal cord shadow in Figure 11 to the outer fringes can be seen, denoting changes in Raman spectra elastic (EE) and inelastic (IE) scattering. These results are only performed on a single, uninjured animal, however, and additional testing and range acquisition for hematocrit levels are needed to confirm the use of Raman spectroscopy as a measure of hematocrit in live rat spinal cords. Additionally, future tests are needed to verify if changes to blood flow can be acquired in injured animals over time. Total acquisition time for a hematocrit scan is approximately 30 minutes depending on the size of the open surgical area and portion of the spinal cord being measured. Measurements similar to those taken previously from other experiments in this thesis showed similar timescales, indicating long timescale measurements of hematocrit levels in the spinal cord after injury are possible. If performed, additional information into localization of blood concentration after contusion injury can be measured and movement of blood concentration during inflammation and healing could be an outcome.

This thesis set out to achieve three separate goals. The first was to develop a method to acquire Raman spectra on live, in vivo rat spinal cords. By comparing the measurement of Raman spectra acquired to previously published work, high similarity in peak location and wavenumbers could be seen in both control and injured animal data. Second, we set out to compare the effects of contusion injury in spinal cord by location and time on in vivo Raman spectra to known literature of spinal cord injury. Comparing both previous work on spinal cord injury using Raman spectra for ex vivo tissue as well as the known immune response to spinal

cord injury in vivo, results were able to verify that changes that were occurring in injured tissue were consistent with those expected due to spinal cord injury. In addition, it was found that cerebrospinal fluid changes are highly dynamic in the timescale immediately after injury, warranting further examination of the interstitial fluid within spinal cord physiology. This also helps to confirm our third goal of comparing changes in specific chemical groups from Raman spectra to known tissue injury response. We can see that changes in bicarbonate levels and phosphorylation levels not previously seen in ex vivo Raman tissue measurements can be acquired using our in vivo method. While the majority of this work acts as a pilot study, the results show great promise that additional work using Raman spectroscopy will find changes throughout timescale of the injury process.

Chapter 5: Conclusions

In conclusion, we demonstrated that Raman spectroscopy can be used in an in vivo surgical environment on live rat models. Measurements collected from the Raman spectra correlate with known spinal cord injury spectra both from our own previous lab experiments and in Raman spinal cord injury literature. To our knowledge, we are the first to demonstrate use of Raman spectroscopy on a live, in vivo spinal cord. Both control and injury animals were used to measure the effects of contusion weight drop on rat spinal cords. Some changes that are shown in both control and injured animals appear to be similar in spectra, indicating that additional, unaccounted damage is occurring. It is hypothesized that these changes may be due to the surgical procedure, the environmental exposure of the tissue, or the Raman laser itself. Despite these artifacts, however, we saw measurable changes between those of injured and control animals attributed to changes seen in cerebrospinal fluid and plasma shown in spinal cord injury literature. Additionally, use of the Raman scanning method was demonstrated to have possible

applications in measuring hematocrit levels in spinal cords using previously demonstrated software. Overall, these data and methods contribute to the use of Raman spectroscopy as a measurement tool for in vivo injury particularly in the area of spinal cord injury and a viable technique to measure early timepoint changes due to contusion injury.

Chapter 6: Future Work

Additional work in perfecting the methodology of acquiring Raman spectra is required for future experiments. Manual focusing of the laser after impact required movement of the laser from its initial z plane height, adding variability to the final focal position of the laser during scanning. By automating the laser focus with a micromotor, similar to the stage used to move the animal, the laser position could be focused initially, the location recorded, and the laser height changed to allow movement of the animal freely without the laser being removed and reattached. In this same vein, automation of moving the impactor rod would also eliminate the need to move the animal along the rails used to align the rod with the spinal impact site. This would also require having the impactor device on rails itself to move above the animal instead, with either a motor to precisely define where the impact would occur, or simple manual rails to align above the impact site if exact precision is not needed.

More experimental Raman spectra from both injury and control animals are required as well, as this study had a subsequently low number of samples, n=3, to make statistical comparisons to. While differences were seen, additional samples to increase the power are required. Using one example of the averages and standard deviations of the subtraction spectra for 1666 cm^{-1} for control and injury for position C, at 80 percent power an additional 3 animals would be required. While this may not be true for all wavenumbers, it does show that additional animals are required to improve the power of the experimental procedure. Additionally, it was

noted earlier that a single injury animal did have a large standard deviation compared to other injured animals. Due to this work involving living animals, a high variability of result is expected and additional experiments to help remove some extraneous outliers would be beneficial.

One change in the future work for this project would be extending the amount of time measuring injury. With up to 5 hours after injury being measured, increasing the time to a range between 5 hours and 1 day to observe a continual change across the course of the day would be a logical continuation of this work. Previous measurements of injury in the spinal cord in our lab using Raman spectroscopy begin at 1 day after injury in the case of scanning organotypic slice cultures of tissue, leaving a gap of knowledge from the early timepoint to 1 day. In addition, measuring Raman changes in vivo much later after injury would help to see changes otherwise unknown, as other methods of using Raman to measure injury require ex vivo or in vitro cultures, removing the effects that the body may have on the tissue in real time. Future experiments using the timepoint method utilized previously our the lab[5] can be compared to previous work. Finally, changing the level of injury could produce different results, as the insult used in this work was set to what is known in spinal cord injury work as a "moderate" level of injury. By increasing or decreasing the level of injury, different levels of change could be observed, and factors such as the efficacy of Raman spectra to detect minor changes can be explored.

References

1. National Spinal Cord Injury Statistics Center. Spinal Cord Injury Facts and Figures at a Glance. The Journal of Spinal Cord Medicine. doi:10.1179/204577211X13218754005537.

2. Sandner B, Puttagunta R, Motsch M, et al. Systemic epothilone D improves hindlimb function after spinal cord contusion injury in rats. *Exp Neurol*. 2018;(January):0-1. doi:10.1016/j.expneurol.2018.01.018.

3. Magaki SD, Williams CK, Vinters H V. Glial function (and dysfunction) in the normal & ischemic brain. *Neuropharmacology*. 2017:1-8. doi:10.1016/j.neuropharm.2017.11.009.

4. Chen C, Zhang YP, Sun Y, et al. An In Vivo Duo-color Method for Imaging Vascular Dynamics Following Contusive Spinal Cord Injury. *J Vis Exp*. 2017;(130):1-10. doi:10.3791/56565.

5. Saxena T, Deng B, Stelzner D, Hasenwinkel J, Chaiken J. Raman spectroscopic investigation of spinal cord injury in a rat model. *J Biomed Opt*. 2011;16(2):027003. doi:10.1117/1.3549700.

6. Bowes AL, Yip PK. Modulating Inflammatory Cell Responses to Spinal Cord Injury: All in Good Time. *J Neurotrauma*. 2014;31(21):1753-1766. doi:10.1089/neu.2014.3429.

7. Obermeyer B, Daneman R, Ransohoff R. Development, maintenance and disruption of the Blood-Brain Barrier. *Nat Med*. 2013;19(12):1584-1596.

8. Rouanet C, Reges D, Rocha E, et al. Traumatic spinal cord injury: current concepts and treatment update. *Arq Neuropsiquiatr*. 2017;75(6):387-393. doi:10.1590/0004-282x20170048.

9. Sofroniew M V. Multiple roles for astrocytes as effectors of cytokines and inflammatory mediators. *Neuroscientist*. 2014;20(2):160-172. doi:10.1177/1073858413504466.

10. Zamanian JLJ, Xu L, Foo LCL, et al. Genomic Analysis of Reactive Astrogliosis. *J …*. 2012;32(18):6391-6410. doi:10.1523/JNEUROSCI.6221-11.2012.Genomic.

11. Adams KL, Gallo V. The diversity and disparity of the glial scar. *Nat Neurosci*. 2018;21(1):9-15. doi:10.1038/s41593-017-0033-9.

12. Hellwig S, Heinrich A, Biber K. The brain's best friend: microglial neurotoxicity revisited. *Front Cell Neurosci*. 2013;7(May):1-11. doi:10.3389/fncel.2013.00071.

13. Ellingson BM, Salamon N, Holly LT. Imaging techniques in spinal cord injury. *World Neurosurg*. 2014;82(6):1351-1358. doi:10.1016/j.wneu.2012.12.004.

14. Ducker TB, Salcman M, Perot PL, Ballantine D. Experimental spinal cord trauma, I: Correlation of blood flow, tissue oxygen and neurologic status in the dog. *Surg Neurol*. 1978;10(1):60-63. http://www.ncbi.nlm.nih.gov/pubmed/684608.

15. Rivlin AS. Regional spinal cord blood flow in rats after severe cord trauma. *J Neurosurg*. 1978;49(6):844-853. doi:10.3171/jns.1978.49.6.0844.

16. Ito T, Oyanagi K, Wakabayashi K, Ikuta F. Traumatic spinal cord injury: a neuropathological study on the longitudinal spreading of the lesions. *Acta Neuropathol*. 1997;93(1):13-18.

17. Dvorak MF, Noonan VK, Fallah N, et al. The Influence of Time from Injury to Surgery on Motor Recovery and Length of Hospital Stay in Acute Traumatic Spinal Cord Injury: An Observational Canadian Cohort Study. *J Neurotrauma*. 2015;32(9):645-654.

doi:10.1089/neu.2014.3632.

18. Krafft C, Popp J. The many facets of Raman spectroscopy for biomedical analysis. *Anal Bioanal Chem*. 2015;407(3):699-717. doi:10.1007/s00216-014-8311-9.

19. Andrews DL. Rayleigh Scattering and Raman Spectroscopy, Theory. In: *Encyclopedia of Spectroscopy and Spectrometry*. Elsevier; 1999:1993-2000. doi:10.1006/rwsp.2000.0260.

20. Cadusch PJ, Hlaing MM, Wade SA, McArthur SL, Stoddart PR. Improved methods for fluorescence background subtraction from Raman spectra. *J Raman Spectrosc*. 2013;44(11):1587-1595. doi:10.1002/jrs.4371.

21. Smith E, Dent G. *Modern Raman Spectrocopy: A Practical Approach*.; 2005. doi:10.1002/0470011831.

22. Stenhouse I a, Williams DR, Cole JB, Swords MD. CARS measurements in an internal combustion engine. *Appl Opt*. 1979;18(22):3819-3825. doi:10.1364/AO.18.003819.

23. Aguilar APM, Lee T, Pattenden L, Yeo L, Friend J, Thomas W. RAMAN SPECTROSCOPY FOR THE DETECTION OF CANCERS AND PRECANCERS. 2018;1(1):3. doi:10.1146/annurev.bioeng.5.011303.120723.

24. Small DM, Sanchez WY, Hickey MJ, Gobe GC. Polarization in Raman spectroscopy helps explain bone brittleness in genetic mouse models. *J Biomed Opt*. 2014;19(2):020901. doi:10.1117/1.

25. Shiyamala Duraipandian, a Mads Sylvest Bergholt, a Wei Zheng, a Khek Yu Ho, b Ming Teh, c Khay Guan Yeoh b J. Real-time Raman spectroscopy for , online gastric cancer diagnosis during clinical endoscopic examination in vivo Shiyamala. *J Biomed Opt*.

2012;17(10). doi:10.1117/1.JBO.17.

26. Motz JT, Gandhi SJ, Scepanovic OR, et al. Real-time Raman system for in vivo disease diagnosis. *J Biomed Opt*. 2005;10(3):031113. doi:10.1117/1.1920247.

27. Jermyn M, Mok K, Mercier J, et al. Intraoperative brain cancer detection with Raman spectroscopy in humans. *Sci Transl Med*. 2015;7(FEBRUARY):274. doi:10.1126/scitranslmed.aaa2384.

28. Vasefi F, MacKinnon N, Farkas DL, Kateb B. Review of the potential of optical technologies for cancer diagnosis in neurosurgery: a step toward intraoperative neurophotonics. *Neurophotonics*. 2016;4(1):011010. doi:10.1117/1.NPh.4.1.011010.

29. Ruberto S. Raman spectroscopic investigation of chondroitinase ABC treatment after spinal cord injury in an organotypic model. 2013:56.

30. Young W. Spinal cord contusion models. *ProgBrain Res*. 2002;137(0079-6123 (Print)):231-255.

31. Sato H, Yamamoto YS, Maruyama A, Katagiri T, Matsuura Y, Ozaki Y. Raman study of brain functions in live mice and rats: A pilot study. *Vib Spectrosc*. 2009;50(1):125-130. doi:10.1016/j.vibspec.2008.09.012.

32. Kast RE, Auner GW, Rosenblum ML, et al. Raman molecular imaging of brain frozen tissue sections. *J Neurooncol*. 2014;120(1):55-62. doi:10.1007/s11060-014-1536-9.

33. Wang S, Liang Z, Gong Y, et al. Confocal raman microspectral imaging of ex vivo human spinal cord tissue. *J Photochem Photobiol B Biol*. 2016;163:177-184. doi:10.1016/j.jphotobiol.2016.08.032.

34. Chaiken J, Deng B, Goodisman J, Shaheen G, Bussjager RJ. Analyzing near-infrared scattering from human skin to monitor changes in hematocrit. *J Biomed Opt*. 2011;16(9):097005. doi:10.1117/1.3625283.

35. Chaiken J, Voss E, Bussjager RJ, Shaheen G. Towards an improved assignment of spectral features in tissue modulated non-invasive Raman spectroscopy of human fingertips. 2007;643004(February 2007):643004. doi:10.1117/12.708010.

36. Li X, Yang T, Li S, Wang D, Song Y, Zhang S. Raman spectroscopy combined with principal component analysis and k nearest neighbour analysis for non-invasive detection of colon cancer. *Laser Phys*. 2016;26(3). doi:10.1088/1054-660X/26/3/035702.

37. Ong YH, Lim M, Liu Q. Comparison of principal component analysis and biochemical component analysis in Raman spectroscopy for the discrimination of apoptosis and necrosis in K562 leukemia cells. *Opt Express*. 2012;20(20):22158. doi:10.1364/OE.20.022158.

38. Shlens J. A tutorial on principal component analysis: derivation, discussion and singular value decomposition. *Int J Remote Sens*. 2003;2:1-16. doi:10.1.1.115.3503.

39. Baker K. Singular value decomposition tutorial. *Ohio State Univ*. 2005;2005:24. doi:10.1021/jo0008901.

40. Andrews H, Patterson III C. Singular value decomposition (SVD) image coding. *IEEE Trans Commun*. 1976;24(4):425-432. doi:10.1109/TCOM.1976.1093309.

41. Krafft C, Neudert L, Simat T, Salzer R. Near infrared Raman spectra of human brain lipids. *Spectrochim Acta - Part A Mol Biomol Spectrosc*. 2005;61(7):1529-1535.

doi:10.1016/j.saa.2004.11.017.

42. Davis AR, Oliver BG. A Vibrational-Spectroscopic Study of the Species Present in the CO2-HzO System. 1972;1(4):329-339.

43. Degen IA, Newman GA. Raman spectra of inorganic ions. *Spectrochim Acta Part A Mol Spectrosc*. 1993;49(5-6):859-887. doi:10.1016/0584-8539(93)80110-V.

44. Frantz JD. Raman spectra of potassium carbonate and bicarbonate aqueous fluids at elevated temperatures and pressures: Comparison with theoretical simulations. *Chem Geol*. 1998;152(3-4):211-225. doi:10.1016/S0009-2541(98)00058-8.

45. Zhang D, Ortiz C, Xie Y, Jo Davisson V, Ben-Amotz D. Detection of the site of phosphorylation in a peptide using Raman spectroscopy and partial least squares discriminant analysis. *Spectrochim Acta - Part A Mol Biomol Spectrosc*. 2005;61(3):471-475. doi:10.1016/j.saa.2004.04.019.

46. Daković M, Stojiljković AS, Bajuk-Bogdanović D, et al. Profiling differences in chemical composition of brain structures using Raman spectroscopy. *Talanta*. 2013;117:133-138. doi:10.1016/j.talanta.2013.08.058.

47. Czamara K, Majzner K, Pacia MZ, Kochan K, Kaczor A, Baranska M. Raman spectroscopy of lipids: A review. *J Raman Spectrosc*. 2015;46(1):4-20. doi:10.1002/jrs.4607.

48. Park Y, Luo T, Zhang F, et al. Downregulation of Src-kinase and glutamate-receptor phosphorylation after traumatic brain injury. *J Cereb Blood Flow Metab*. 2013;33(10):1642-1649. doi:10.1038/jcbfm.2013.121.

49. Sakka L, Coll G, Chazal J. Anatomy and physiology of cerebrospinal fluid. *Eur Ann Otorhinolaryngol Head Neck Dis*. 2011;128(6):309-316. doi:10.1016/j.anorl.2011.03.002.

50. Di Terlizzi R, Platt S. The function, composition and analysis of cerebrospinal fluid in companion animals: Part I - Function and composition. *Vet J*. 2006;172(3):422-431. doi:10.1016/j.tvjl.2005.07.021.

51. Ohashi T, Morimoto T, Kawata K, Yamada T, Sakaki T. Correlation between spinal cord blood flow and arterial diameter following acute spinal cord injury in rats. *Acta Neurochir (Wien)*. 1996;138(3):322-329.

52. Florence CM, Baillie LD, Mulligan SJ. Dynamic Volume Changes in Astrocytes Are an Intrinsic Phenomenon Mediated by Bicarbonate Ion Flux. *PLoS One*. 2012;7(11):1-9. doi:10.1371/journal.pone.0051124.

53. Ye S, Li H, Yang W, Luo Y. Accurate determination of interfacial protein secondary structure by combining interfacial-sensitive amide i and amide III spectral signals. *J Am Chem Soc*. 2014;136(4):1206-1209. doi:10.1021/ja411081t.

54. Yang W-J, Chen W, Chen L, et al. Involvement of tau phosphorylation in traumatic brain injury patients. *Acta Neurol Scand*. 2017;135(6):622-627. doi:10.1111/ane.12644.

55. Garai E, Sensarn S, Zavaleta CL, et al. High-sensitivity, real-time, ratiometric imaging of surface-enhanced Raman scattering nanoparticles with a clinically translatable Raman endoscope device. *J Biomed Opt*. 2013;18(9):096008. doi:10.1117/1.JBO.18.9.096008.

56. Bosmia AN, Hogan E, Loukas M, Tubbs RS, Cohen-Gadol AA. Blood supply to the human spinal cord: Part I. Anatomy and hemodynamics. *Clin Anat*. 2015;28(1):52-64.

doi:10.1002/ca.22281.

57. TSUBOI M, EZAKI Y, AIDA M, et al. Raman Scattering Tensors of Tyrosine. *Nucleic Acids Symp Ser*. 1997;(37):61-71. doi:10.1002/(SICI)1520-6343(1998)4:1<61::AID-BSPY7>3.0.CO;2-V.

58. Conlay LA, Maher TJ, Roberts CH, Wurtman RJ. Effects of hemorrhagic hypotension on tyrosine concentrations in rat spinal cord and plasma. *Neurochem Int*. 1988;12(3):291-295. doi:10.1016/0197-0186(88)90167-2.

59. Farrar MJ, Rubin JD, Diago DM, Schaffer CB. Characterization of blood flow in the mouse dorsal spinal venous system before and after dorsal spinal vein occlusion. *J Cereb Blood Flow Metab*. 2015;35(4):667-675. doi:10.1038/jcbfm.2014.244.

60. Wu TC, Vasudev M, Dutta M, Stroscio MA. Raman and surface-enhanced raman scattering (SERS) studies of the thrombin-binding aptamer. *IEEE Trans Nanobioscience*. 2013;12(2):93-97. doi:10.1109/TNB.2013.2242484.

61. Boknäs N, Faxälv L, Centellas DS, et al. Thrombin-induced platelet activation via PAR4: Pivotal role for exosite II. *Thromb Haemost*. 2014;112(3):558-565. doi:10.1160/TH13-12-1013.

VITA

Kyle Bishop

Educational History

Master of Science in Bioengineering from Syracuse University, New York, August 2018.
Thesis Title: "*In vivo, real-time spectroscopic assessment of contusion-based spinal cord injury in a rat model"*

Bachelor of Science in Bioengineering from Binghamton University, New York, May 2014.

Associate of Science in Individual Studies from State University of New York Ulster, New York, May 2011.

Academic Employment

Graduate Teaching Assistant, Department of Biomedical Engineering, Syracuse University August 2014-May 2017. Acted as Mentor, Grader and Assistant to courses including Mass and Energy Balance, Computational Tools for Engineers, and Biomechanics.

Graduate Research Assistant, Department of Biomedical Engineering, Syracuse University August 2014-August 2018. Acted as lab manager with responsibilities including management of chemical inventory, management of cell culture space and maintaining cultures for lab and ordering materials.

Conference Proceedings

Fillioe S., Bishop K., Tun S., Dent P., Deng B., Peterson C.M., Goodisman J., Hasenwinkel J., Chaiken J. "*A chemist's view of inflammation in contusion injured spinal cord in a rat model: noninvasive, noncontact, in vivo Raman spectroscopy at very early times after injury*" SPIE 2019 Submission, *In Progress*

Fillioe S., Bishop K, Kim J., McDonough R., Ortiz S., Goodisman J., Hasenwinkel J., Chaiken J. *"In vivo, noncontact, real-time, optical and spectroscopic assessment of the immediate local physiological response to spinal cord injury in a rat model"* 2017 submission, SPIE 2018 acceptance. *Publication in Progress*

Memberships and Certifications

Phi Theta Kappa

Description: Honors Society for 2 Year Collages obtained from SUNY Ulster. Required a 3.75 GPA or above for admission. Maintained throughout career in SUNY Ulster. Graduated with honors.

Biomedical Engineering Society (BMES)

Description: Professional society associated with Biomedical Engineering.

NIH Protecting Human Research Participants Certificate

Description: Certificate used to show completion of training for interaction with human subjects for research from the National Institute of Health. Obtained Fall 2012.

Spinal Cord Contusion Injury Certification Training Certificate

Description: Certification obtained from Rutgers University, W.M. Keck Center for Collaborative Neuroscience, New Jersey, for use with their approved spinal cord impact device. Training included spinal cord surgery, blood acquisition, humane euthanasia, animal care prior to and after injury and contusion-based injury.

Integrative Graduate Education and Research Traineeship (IGERT) Fellow

Description: Accepted fellowship given for two years from Fall 2016-Spring 2018. Member statement included the promotion of collaborative research initiatives between various fields and the promotion of new graduate scientists.